Absorption and dispersion spectroscopy in the far infra-red region

James, Peter Leslie

UNIVERSITY OF DURHAM

A Thesis entitled

ABSORPTION AND DISPERSION SPECTROSCOPY IN THE FAR INFRA-RED REGION

submitted by

Peter Leslie James, B.Sc.

A candidate for the degree of Master of Science 1976

TO MY PARENTS

MEMORANDUM

The work described in this thesis was carried out in the University of Durham between September 1975 and September 1976. This work has not been submitted for any other degree and is the original work of the author, except where acknowledged by reference.

ACKNOWLEDGEMENTS

I am grateful to Professor D.H. Martin, Dr. P. Ade and Mr. E. Puplett of Queen Mary College, London, for their help and advice during the installation and testing of the cooled detector and polarising system. I am also grateful to Beckman-RIIC, for their financial support during this work and in particular to Mr. W.A. Scott for his guidance and encouragement. My thanks are due to Dr. M.J. Morant and Mr. J. Gibson of our Applied Physics Department for their help with recoating our refractive index cell. I would also like to thank Mr. R. Brown and Mr. G. Rowe of this department who have given invaluable advice on the instrument electronics and modifications. I am grateful to Dr. A. Royston for writing the minicomputer program for processing our data and for his advice on many other computing problems.

Finally I wish to thank my Supervisor, Dr. J. Yarwood, for his constant encouragement and advice, Mr. D. Hartshorn for the photography and Mrs. B.A. McGonigle for typing this thesis.

Abstract

The work described in this thesis can be divided into two main parts. The first part describes the modifications of the instrument (a Beckman-RIIC FS720) to enable it to be operated in the polarising mode with a liquid helium cooled detector. Several problems were encountered during the testing of this equipment particularly when operating the polarising system. Initially the spectra recorded with this system showed considerable distortion in the high and low frequency regions. The low frequency distortion was found to arise from electrical non-linearity (due to overload) within the electronics (RIIC FS200) and modifications to the amplifier have eliminated this problem. The high frequency distortion, which appears as a ≈ 120 cm^{-1} limit, has not been corrected and is now thought to arise from a 'software' (computing) problem.

The signal-to-noise ratio tests carried out on the cooled detector indicate that the bolometer element may not be operating at its most sensitive temperature due to overheating by the hot source. However, when operating with heavy optical filtering (therefore reducing the radiation reaching the bolometer) it has been possible to record spectra in the very far-infrared region ($20 \rightarrow 5$ cm^{-1}).

The second part of the thesis describes the practical operation and tests carried out on the previously constructed cell designed for conversion of the instrument to operate in the dispersive mode. To enable this cell to be mounted vertically on the instrument a top window has been included to hold a liquid sample. This leads to the appearance of reflections and multiple reflections not present when studying a gravity held liquid. These reflection fringes have been

fully assigned and therefore it has been possible to obtain the continuous dispersion (refractive index) curve of a liquid in the far-infrared region.

The overall aim of this work has been to test the limitations and accuracy of the new equipment and make original studies in the far-infrared region.

Contents

Diagrams and Tables

CHAPTER I

a) Objectives of the Work

The aim of this work is to improve the standard instrument, a Beckman -RIIC FS720 interferometer, with the addition of a new optical system and a fast detector. The detector chosen was a Germanium bolometer operating at low temperature which should extend the frequency range down to about 2 cm^{-1} (60 GHz) and therefore provide some continuity with the microwave region. It is also possible to study optically thicker, more absorbing samples by taking advantage of the improved signal to noise ratio of the bolometer over the standard golay.

The optical system has been changed to the polarising configuration described by Martin and Puplett.[1] The advantage of this system over the conventional system is that it provides a greater energy throughput, with an improvement in signal to noise ratio, and gives a flatter background over the frequency range observed (which extends from about 2 → 150 cm^{-1}). The third piece of equipment used in this work is the previously constructed cell for the operation of the interferometer in the dispersive mode.[2] Combined with the low frequency (long wavelength) detector the new cell will provide continuous refractive index data into the far-infrared region not previously studied.

The overall aim of the work described in this thesis has been to test and assess the merits and accuracy of the new equipment and make original studies into the very far-infrared region (2 - 30 cm^{-1}).

b) Value of Low Frequency Measurements

The far-infrared region may be used to study ion-molecule interactions[3,4] of which there are many examples in the field of biochemistry, where the extra sensitivity of the modified instrument can be used to study systems in their natural but highly absorbing medium of water.[10] Such applications include the study of the Mg^{2+} ion and the transport control mechanism across the cell wall of bacteria.[5,6,7] The biosynthetic emzymes, found in the phospholipid membrane of bacterial cell are Mg^{2+} dependent and it has been shown that the teichoic acid in the outer cell

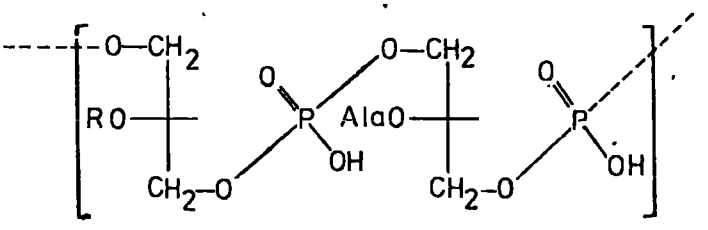

R = H or glycosyl , Ala = alanyl .

A typical glycerol teichoic acid

wall has some control over the concentration of Mg^{2+} reaching the phospholipid membrane of the inner cell wall.[8,9] The exact nature(s) and site(s) of binding of the Mg^{2+} ion to the teichoic acid is not known, but it may be possible to study the effect of Mg^{2+} or other ions on the cell wall material in the far-infrared region. Other possibilities include the study of Mg^{2+} rattling in a solvent cage, possibly in aqueous or other highly polar solvent media and the study of structure perturbation of water when Mg^{2+} or Ca^{2+} are added.

c) The Michelson Interferometer

A Michelson interferometer can be represented very simply as shown in Fig. 1.1.

Radiation from the source s is collimated by either a lens or a system of mirrors at p. The 'parallel' beam of radiation then strikes the beam splitter B and in an ideal case will be 50% reflected and 50% transmitted. After reflection at the two mirrors M_1 and M_2 the two beams are recombined at B where intensity division occurs again and the resulting wave is brought to a focus on the detector D by the mirror or lens system Q. In use the mirror M_2 is moved to the position M_2' and the beam in that arm of the interferometer undergoes a phase shift associated with the path difference x between beams (1) and (2). , where the path difference x is equal to twice the mirror displacement. When M_2 is in such a position that distance B - M_1 is equal to the distance B - M_2., the beams will recombine at B coherently and give a maximum intensity I(o) of radiation at the detector D, hence this position is referred to as zero path difference (Z.P.D.).

Now if we assume that the source s is monochromatic at frequency $\bar{\nu}$ the intensity I(x) at a position x, displaced from the zero path difference will be given by[11]

$$I(x) = I(o)\mathrm{Cos}(2\pi\bar{\nu}x) \qquad 1.1$$

and an interference pattern such as figure 1.2a will be detected by D as M_2 is moved and x is increased.

In practice a polychromatic source is used and the interference pattern observed is merely the result of superposition of many curves to

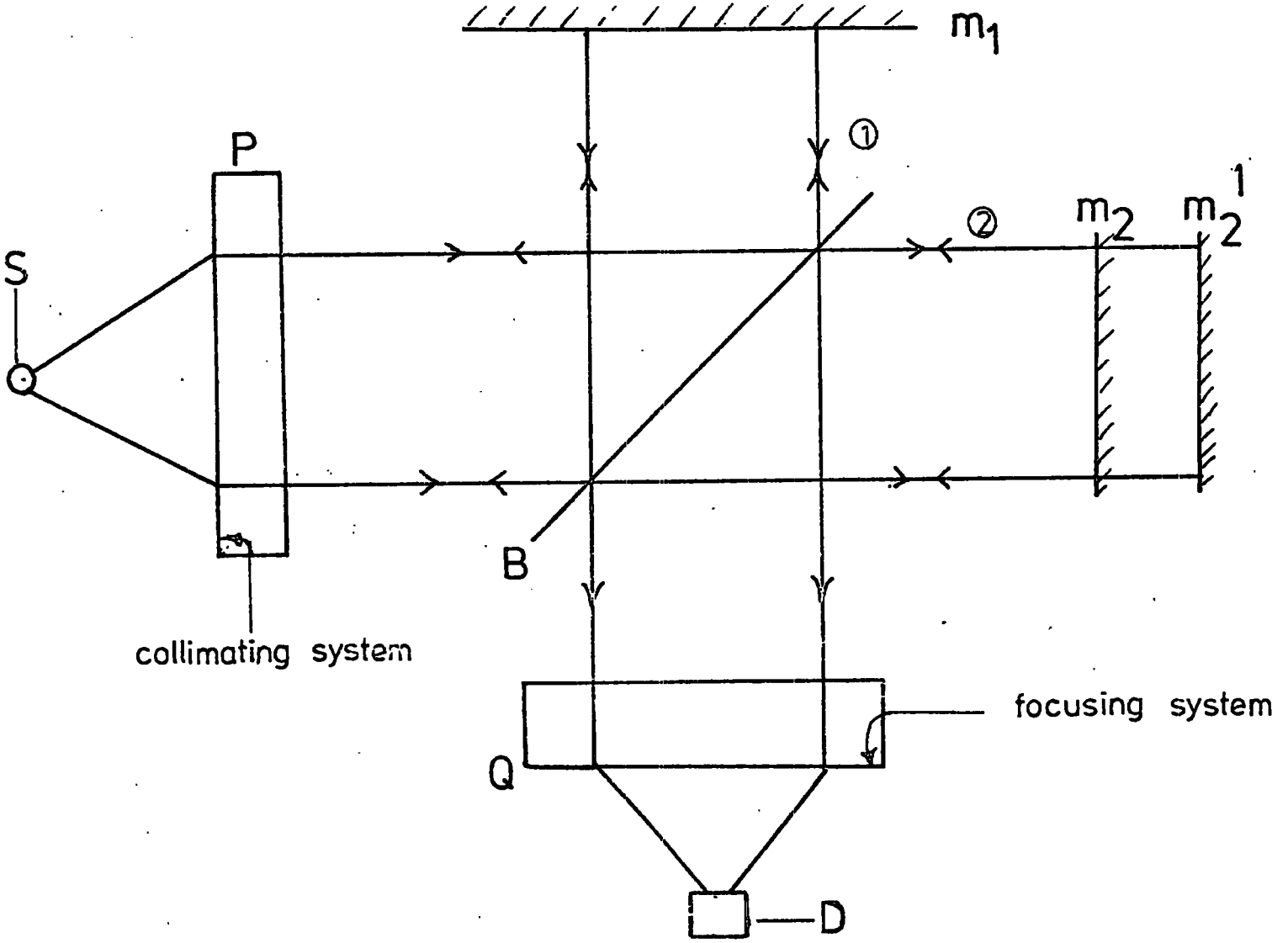

Fig. 1.1 Schematic diagram of a Michelson Interferometer

Fig. 1.2

a) Interference pattern from a monochromatic source

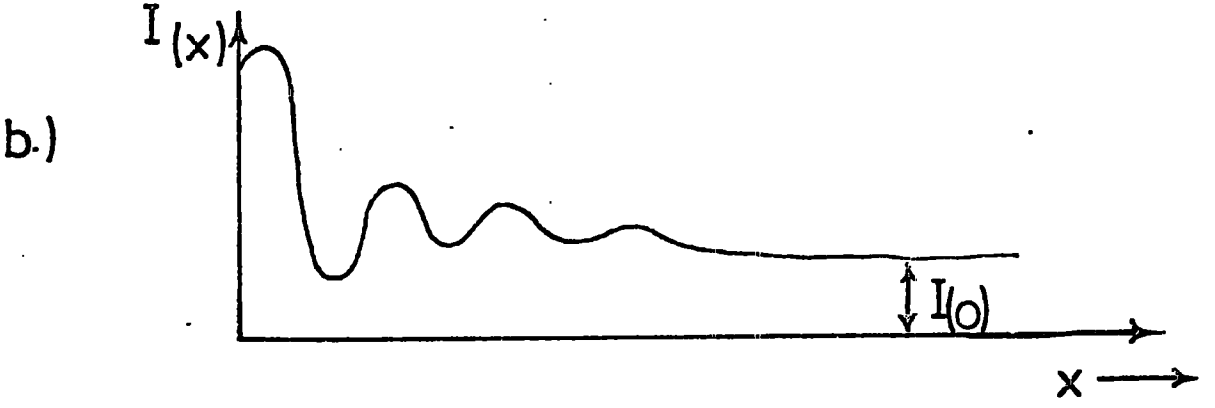

b) Interference pattern from a polychromatic source

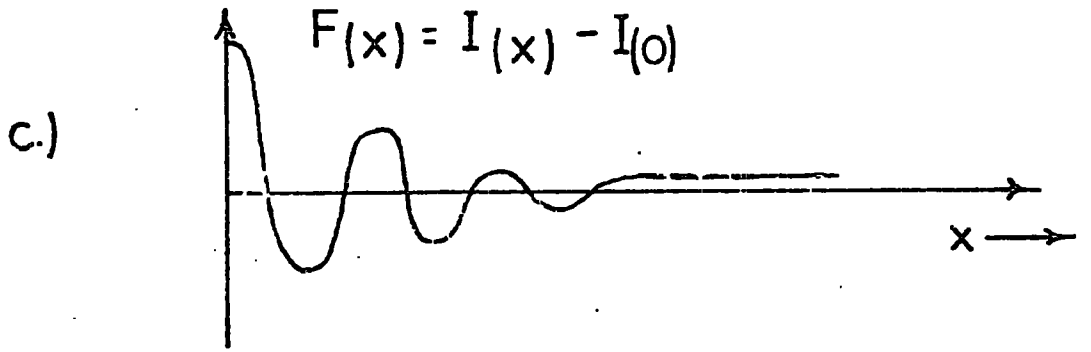

c) A power interferogram

give a pattern as in 1.2b which tends to flatten off at large values of x. This interference pattern is composed of a frequency independent part I(o) and an x dependent part F(x). F(x) is known as the power interferogram and is the interference function I(x) minus I(o). F(x) is represented by figure 1.2c. The form of the power interferogram is

$$F(x) = \int_{-\infty}^{+\infty} B(\bar{\nu}) \text{ Cos } 2\pi \bar{\nu} x d\bar{\nu} \qquad 1.2$$

where $B(\bar{\nu})$ is the intensity as a function of frequency i.e. the spectrum. The frequency and delay time, and the related quantities path difference x and frequency, are conjugate variables. Therefore, the power interferogram is simply a spectrum where the independent variable is time[11] which is the reciprocal of frequency instead of frequency itself. This means that the power interferogram F(x) and the detected spectral power $B(\bar{\nu})$ are a Fourier Transform pair and hence an inversion of Equation 1.2 can be made by Fourier's Integral Theorem to obtain Equation 1.3, where intensity is expressed as a function of frequency in terms of the measurable parameter F(x)

$$B\bar{\nu} = \int_{-\infty}^{+\infty} F(x) \text{ Cos } 2\pi \bar{\nu} x dx \qquad 1.3$$

Thus the spectrum can be recovered from the interferogram.[12]

The limits of the integral obviously cannot be infinite and the upper limit of equation 1.3 is set by x_{max}, the maximum path difference (i.e. twice the mirror displacement). If we then assume that the interferometer introduces no other phase shifts apart from the mirror displacement, the interferogram is symmetrical about zero path difference and equation 1.3 can be rewritten as

$$B(\bar{\nu}) = 2\int_{o}^{x_{max}} F(x) \text{ Cos } 2\pi \bar{\nu} x dx \qquad 1.4$$

The limiting of x to a finite value means that we have set a finite resolution limit in the calculated spectrum. The limiting condition for the resolution $\Delta\bar{\nu}$ of a spectral feature is approximately given by eqn. 1.5

$$\Delta\bar{\nu} = \frac{1}{x_{max}} \qquad 1.5$$

where x_{max} is the total distance travelled from Z.P.D.

Apodisation

The spectra which is calculated from a truncated interferogram may have undesirable spurious features.[13] This is because sharp lines are associated with subsidiary maxima which may be taken for real spectral features. To eliminate this problem a weighting function is applied to the interferogram data such that the intensity falls to zero at x_{max}. The introduction of this apodising function further limits the theoretical resolution to

$$\Delta\bar{\nu} \approx \frac{2}{x_{max}} \qquad 1.6$$

The intensity data of the interferogram is recorded at regular intervals of path difference Δx up to the limit $N\Delta x = x_{max}$ where N is an integer.

The finite value of Δx sets an upper frequency limit of the spectral window because the highest frequency present must be sampled at least once every half cycle. The upper frequency limit $\bar{\nu}_{max}$ is given by equation 1.7.

$$\bar{\nu}_{max} = \frac{1}{\Delta x.2} \qquad 1.7$$

The replacement of a continuous function by a regularly sampled one means that equation 1.4 can be replaced by a summation (eqn. 1.8) which leads to errors in the calculation of the spectrum. This includes phase

$$B(\bar{\nu}) = 2 \sum_{0}^{N} F(x)\ \mathrm{Cos}(2\pi\bar{\nu}x\Delta x)dx \qquad 1.8$$

errors and the occurrence of a phenomenum known as 'aliasing'.

Aliasing

If the interferogram F(x) was a pure cosine function of frequency $\bar{\nu}_o$ then no other wave would pass through all the points sampled and hence the summation given by equation 1.5 would accurately recover the spectral function $B(\bar{\nu})$ near $\bar{\nu}_o$.

However, in the real case an infinite number of higher frequency waves will pass through the sampled points in the observed range if their frequencies satisfy the condition.

$$\bar{\nu}_{\ell} = \nu_o + {}^{\ell}/2\Delta x \qquad 1.9$$

where ℓ = integer 1,2,3,4 ----

The summation 1.8 will then only give true spectral information in the frequency range $0 \rightarrow {}^{1}/2\Delta x$ and then the pattern will repeat itself. This is known as 'aliasing' and restricts the width of spectral band which can be observed. For this reason filters are used to cut out all frequencies above the aliasing frequency. The appearance of an aliasing spectrum is shown in figure 1.3.[2]

Phase Errors

Phase errors arise from instrumental imperfections and the fact that a finite sampling interval means that the exact zero path difference may not be sampled when digitising the interferogram. This problem is obviously less if the sampling interval is made smaller but the error is normally corrected for in the computing of the spectrum by a process

known as autocorrelation. The error due to instrument imperfections is easily overcome by the subtraction of a background spectrum from the sample spectrum (possible because instrument phase error is constant).

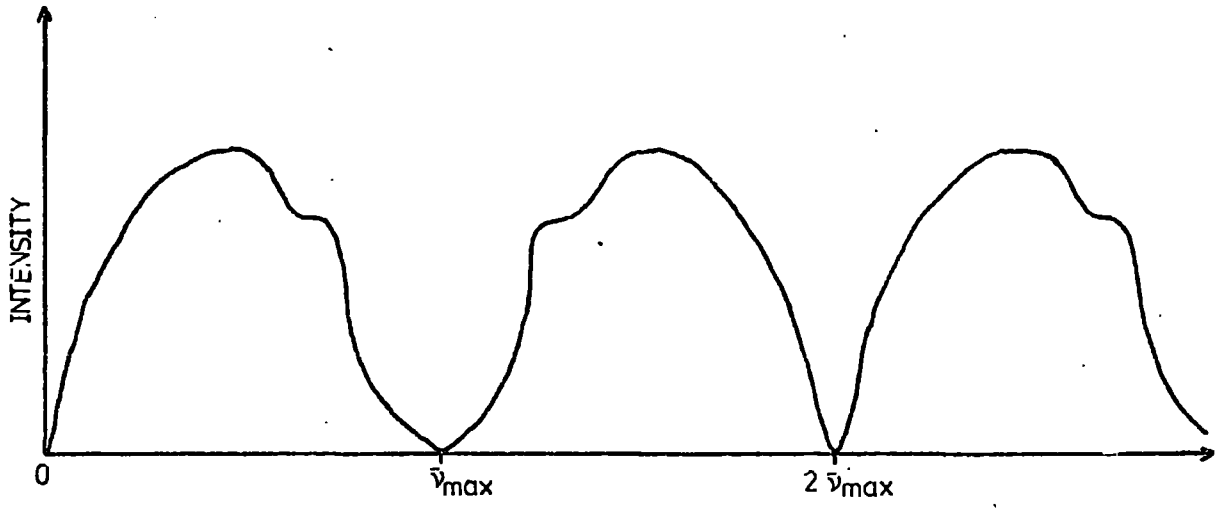

Fig. 1.3 Diagram of an aliasing spectrum

d) Instrumental

The theoretical advantages and disadvantages of interferometers are well known.[14] However, the disadvantages which particularly affect the work on the systems described in section 1(b) are pointed out below.

Disadvantages of the Conventional FS 720 system

The detector in the conventional system (Beckman R11C FS 720) is a Pye Unicam SP.50 Golay cell which, being a mechanical device operates at the relatively low frequency of $12.5H_Z$. The signal-to-noise ratio (S/N) obtained using the Golay cell effectively limits the maximum resolution possible (see page 14.) and makes the study of spectra run in highly absorbing solvents (where the signal is low and hence S/N low) difficult.

The Golay cell sensitivity falls off rapidly below 20-25 cm^{-1} and in practice this means that reliable spectra cannot readily be obtained below 20 cm^{-1}.

The mylar beam splitter of the conventional FS 720 gives rise to two disadvantages. The more serious of the two is the fact that half of the total source energy is reflected/transmitted back to the source and therefore never reaches the sample. This is obviously most unfavourable when studying highly absorbing samples.

The second disadvantage is that each beam splitter is efficient in only limited ranges due to interference within the mylar itself. (See Fig. 1.4). This means that a broad spectral band has to be studied by making several runs with different thickness beamsplitters and the results then have to be matched together.

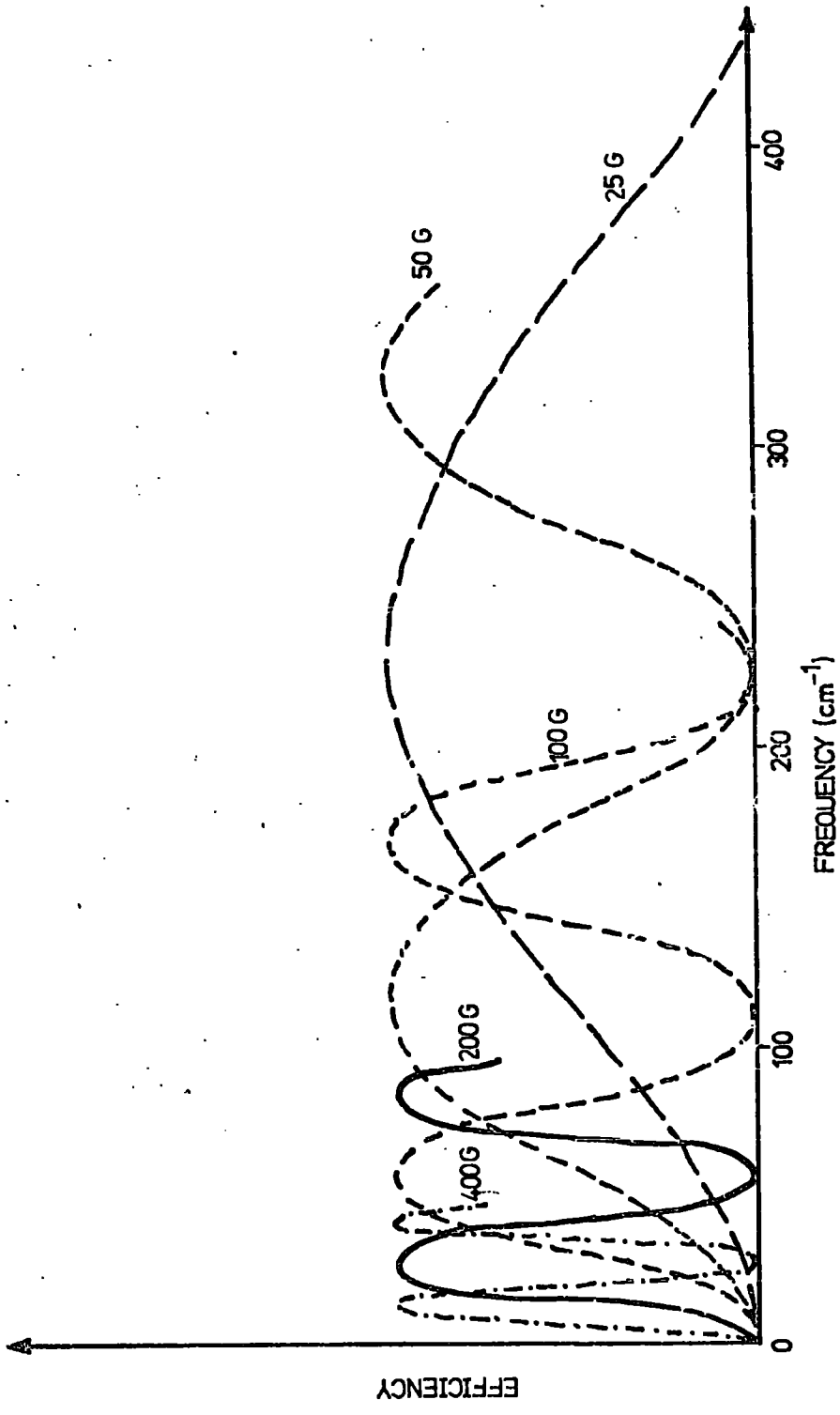

Fig. 1.4 Relative beam splitter efficiencies

When dealing with strongly absorbing samples high resolution is necessary to identify relatively small spectral features. The standard FS 200 electronics with long tune constants (min $\frac{1}{2}$ sec) and short sampling interval (the punch is also a limiting factor here)mean that a high resolution (≈ 1 cm^{-1}) run of a background and sample will take up to one and a half hours.

Finally the conventional system detects an interference pattern about a d.c. 'mean' level. This d.c. level has a noise level associated with it which will be in addition to all other noise sources.

Practical Operation

The optical system of the Beckman-R11C FS 720 interferometer is shown in Figure 1.5.

The mirror drive on the 720 module covers a distance of $\pm$ 5 cm from the zero path position. This means that the maximum path difference over which an interferogram can be recorded is $\pm$ 10 cm. This corresponds to a theoretical resolution of 0.1 cm^{-1} according to equation 1.5, if we assume that the interferogram is not weighted with an apodising function. The use of an apodising function reduces the resolution to 0.2 cm^{-1} as given by equation 1.6. All the interferograms recorded in this work were apodised before the spectrum was calculated.

Application of equation 1.10^{15} imposes a theoretical limit on the

$$R = \frac{2\pi}{\Omega} \approx 8\left(\frac{f}{d}\right)^2 \qquad 1.10$$

where d = source diameter

Ω = solid angle sublended to source

f = focal length of collimating system

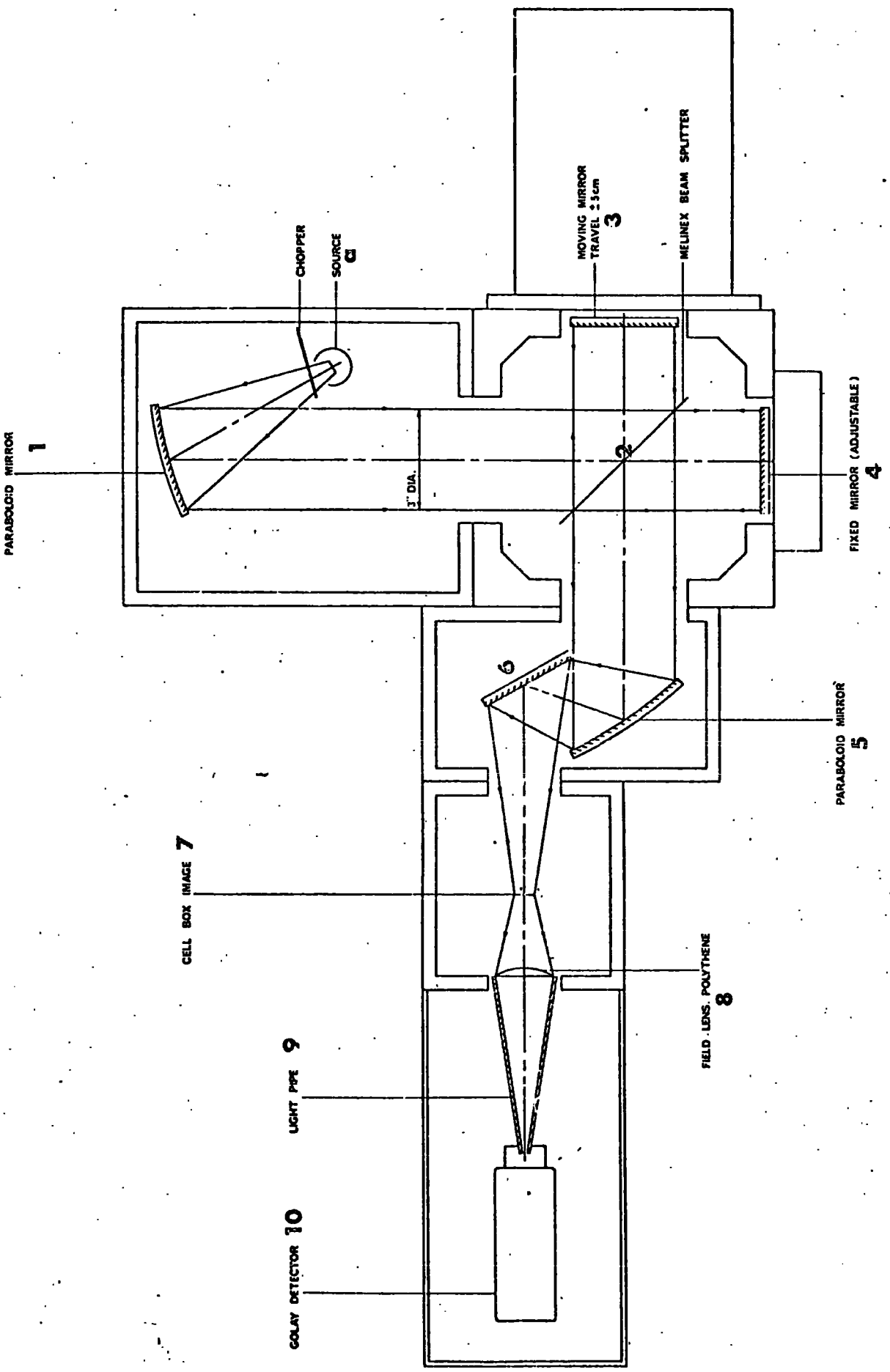

Fig.15. RAY DIAGRAM FOR R.I.I.C. MODULAR FOURIER SPECTROPHOTOMETER FS-720

resolution of an interferometer due to the source size. The source of the FS 720 has a facility for providing apatures of 10 mm, 5 mm and 3 mm which gives resolving powers, R, of 10^3, 4×10^3 and 10^4 respectively, where

$$R = \frac{\bar{\nu}}{\Delta\bar{\nu}} \qquad 1.11$$

Thus it is necessary when choosing the apature size to consider what resolution $\Delta\bar{\nu}$ is required at frequency $\bar{\nu}$.

The most critical factor limiting the resolution in an interferometer is the signal to noise ratio. Nothing will be gained by scanning an interferogram beyond the point at which the real interference level falls to that of the noise level. For this reason most of the interferograms recorded in this work were computed over a path difference of 8.192×10^{-1} cm (i.e. 4.096×10^{-1} cm from zero path difference) which after apodisation gives a theoretical maximum resolution of 2.44 cm^{-1} by application of Equation 1.5.

With the FS 720 interferometer it is possible to sample at every 8μ or 4μ interval. This sets the possible upper frequency limits to 625 cm^{-1} and 1250 cm^{-1} respectively according to Equation 1.7. The interferograms recorded were all sampled at 8μ intervals and black polythene was used to cut out frequencies above the aliasing frequency. In most cases additional filters were used to limit the frequencies falling on the detector to those of interest. The restriction of the optical bandwidth of the background effectively improves the dynamic range of the instrument.[16] Some characteristics of typical filters used are shown in Figure 1.6.

To eliminate noise problems associated with d.c. detection the signal in the FS 720 is modulated periodically at a frequency of 12.5H_Z by a rotating sectored disc. A synchronous a.c. amplifier (FS 200

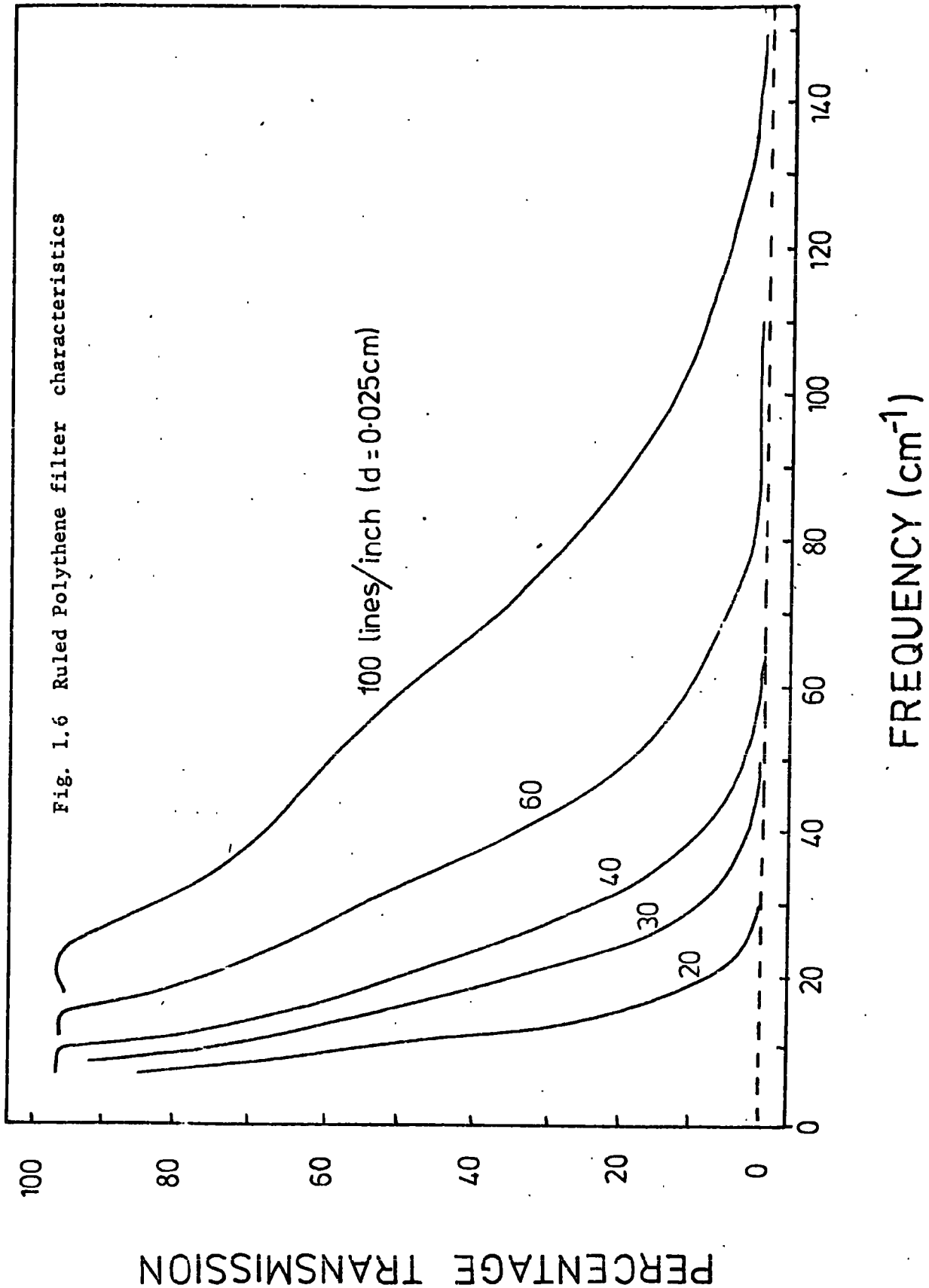
Fig. 1.6 Ruled Polythene filter characteristics
100 lines/inch (d = 0·025cm)
60
40
30
20
PERCENTAGE TRANSMISSION
FREQUENCY (cm⁻¹)
0
20
40
60
80
100
120
140

is phased in to the periodic signal by the pulse from a magnetic reed switch which is triggered by the rotating 'chopper' disc. The resulting interferogram remains symmetric in the ideal case.

CHAPTER II The Cooled Detector and Polarising Optics

a) Theoretical background i) The Cooled Detector

The bolometer was first used as an infrared detector by Langley in 1880. This early form of bolometer was constructed as shown in Fig. 2.1, and can be used as an example to study some basic principles of the bolometer as a detector.[17]

The arrangement is such that two blackened strips of metal, in this case platinum, form part of a wheatstone bridge circuit. The strips are kept as close together as is possible whilst exposing only (a) to the incoming radiation, this is to ensure that both strips are at the same ambient temperature. The bridge circuit is then balanced with only background radiation falling on (a). During operation excess radiation falling on (a) causes a small rise in temperature and subsequently a change in resistance of ΔR. An increase in temperature of a conductor is associated with a decrease in resistance and (a) will then have the resistance of $R-\Delta R$ where R was the ambient resistance. This decrease in resistance causes an unbalance in the bridge circuit which is indicated by a deflection on the galvanometer G.

The change in resistance, ΔR, when a bolometer element is heated is dependent on a quantity called the temperature coefficient of resistance, α, given by equation 2.1.

$$\alpha = \frac{1}{R}\frac{dR}{dT} \qquad 2.1$$

R = resistance of temperature T

The resistance of most metals is proportional to the temperature so, α is given by

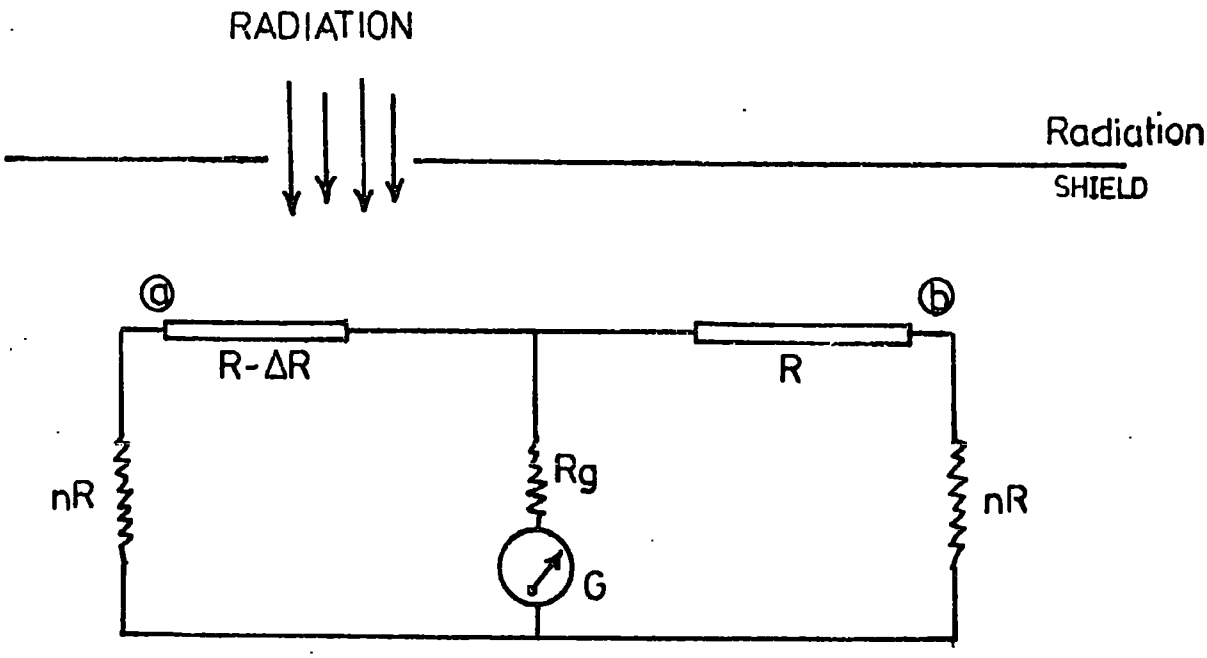

Fig. 2.1 Bolometer arrangement as used by Langley(1880)

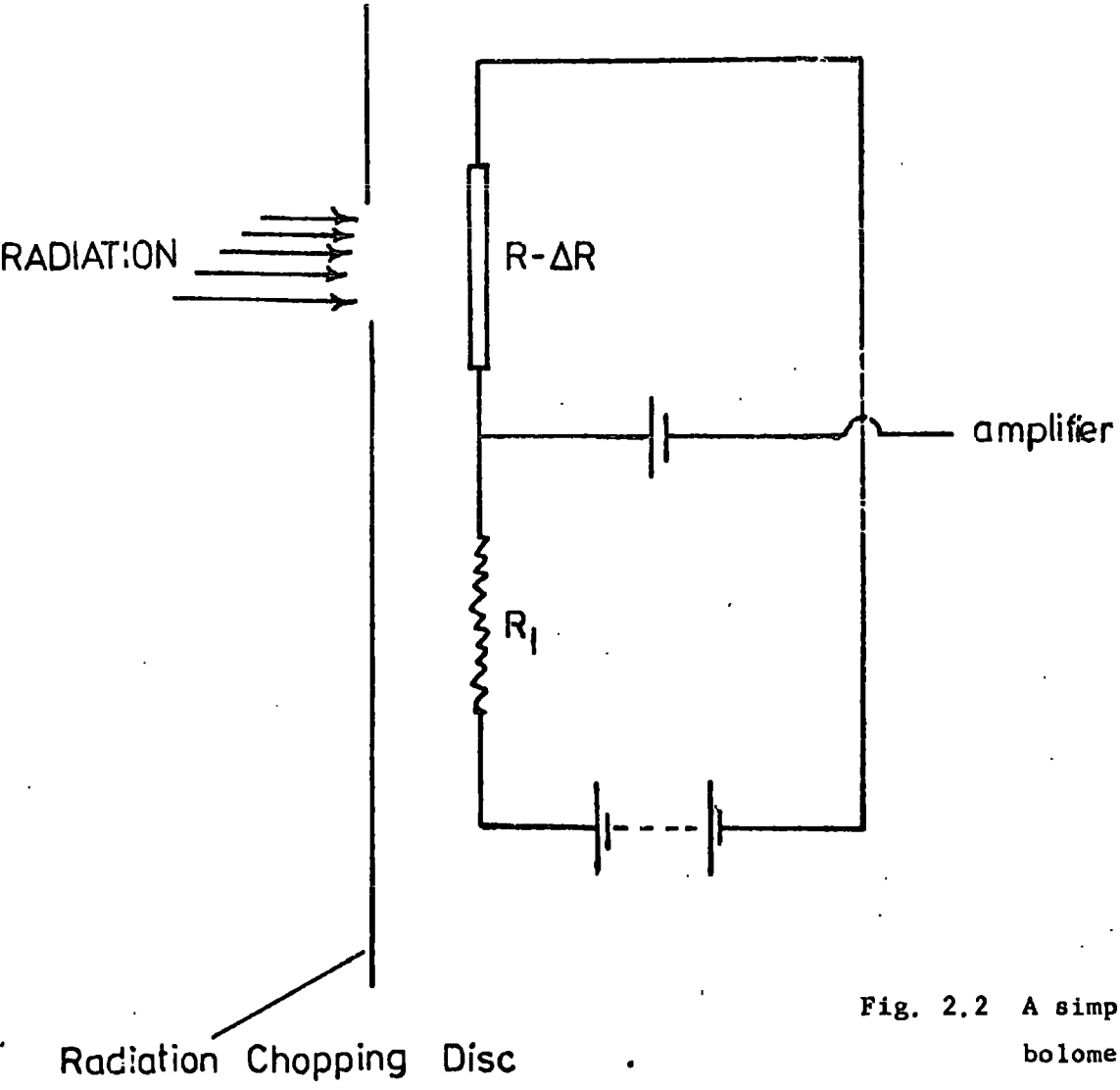

Fig. 2.2 A simple single element bolometer circuit for a.c. operation

$$\alpha = T^{-1} \qquad 2.2$$

Semiconductors, such as doped Germanium, follow the equation

$$R = R_o e^{A/T} \qquad 2.3$$

Where A is a positive constant then

$$\alpha = -A/T^2 \qquad 2.4$$

The change of resistance ΔR for a change in temperature ΔT can be expressed in terms of α as

$$\Delta R = \alpha R \Delta T \qquad 2.5$$

The circuit shown in figure 2.2 is a single element bolometer for ac operation, this circuit will be used to illustrate the calculation of the out of balance current, voltage and a function known as the 'responsivity' r.

Let E be the emf of a battery supplying the steady current through R and R_1. When radiation falls on R the change in resistance of R to $R - \Delta R$ is observed as a change in voltage across the load resister R_1. This voltage change is given by equation 2.6.

$$\Delta v = Fi\Delta R \qquad 2.6$$

where i is the steady exciting current and F is the bridge factor given by

$$F = R_1/(R + R_1) \qquad 2.7$$

For a given value of i the maximum voltage change is obtained when F = 1 that is when $R_1 >> R$.

When calculating the temperature of the element the heating contribution of the constant current i must be included. If the heating power from the current is W_h and the heating power from the radiation falling on the bolometer is ΔW (power absorbed) we can write

$$c \frac{dT}{dt} + G_o (T - T_o) = W_h + \Delta W \qquad 2.8$$

T_o = ambient temperature

T = bolometer temperature

c = thermal capacity of element

G_o = average thermal conductance

Under the steady state where $\Delta W = 0$ we can rewrite equation 2.8 as

$$G_o (T - T_o) = W_h \qquad 2.9$$

If the temperature of the bolometer element is $T + \Delta T$ we can write

$$c \frac{d\Delta T}{dt} + G\Delta T = \frac{dW_h}{dT} \Delta T + \Delta W \qquad 2.10$$

where G = thermal conductance for small temperature changes

The rate of change of W_h with T depends on the circuit arrangement and is given by

$$\frac{dW_h}{dT} = \alpha(T - T_o)G_o \left[\frac{R_1 - R}{R_1 + R}\right] \qquad 2.11$$

Equation 2.10 can then be rewritten in the form

$$c \frac{d\Delta T}{dt} + Ge\Delta T = \Delta W \qquad 2.12$$

where Ge is the effective thermal conductance.

From equation 2.12 it can be seen that the bolometer will be unstable and continue to heat up if $Ge < 0$ when $\Delta W = 0$. For stability of a bolometer we can write

$$\alpha(T + T_o) < 1 \qquad 2.13$$

which for a classical metal, where $\alpha = T^{-1}$ reduces to

$$(T - T_o) < T \qquad 2.14$$

and for the semiconducting bolometer element, where $\alpha = -A/T^2$, reduces to

$$-A(T - T_o) < T^2 \qquad 2.15$$

Expressing equation 2.13 as

$$\frac{dR}{dT} < \frac{R}{T - T_o} \qquad 2.16$$

the stability condition for a bolometer can be represented graphically by plotting R vs T as shown in figure 2.3.[17]

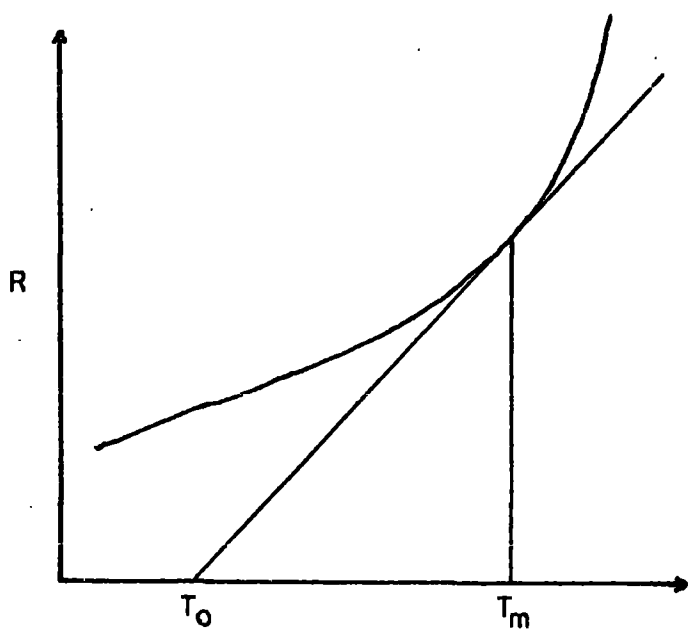

Fig. 2.3 Theoretical stability condition for a bolometer

When T_o is fixed the maximum value of T is given by the tangent drawn from T_o onto the curve as shown. If T is fixed the reverse of this process can be applied to give the minimum permissible value of T_o.

The responsivity, r, of a bolometer is the ratio of the open circuit voltage Δv across the load (figure 2.2) against the change in amplitude, ΔW, of the radiation power falling on the bolometer element. The responsivity of an ac circuit such as figure 2.2. is given by

$$r = \frac{F \epsilon i R \alpha}{G_e (1+\omega^2 \tau^2)^{\frac{1}{2}}} \qquad 2.17$$

where ϵ = effective emissivity and $\tau = C/Ge$

when $R_1 >> R$

$$r = \frac{\epsilon i R \alpha}{(Ge^2+\omega^2 C^2)^{\frac{1}{2}}} = \frac{\epsilon \alpha R^{\frac{1}{2}} (T-T_o)^{\frac{1}{2}} G_o^{\frac{1}{2}}}{(Ge^2+\omega^2 C^2)^{\frac{1}{2}}} \qquad 2.18$$

From equation 2.18 it can be seen that r is proportional to the temperature coefficient of resistance α, the exciting current i, the resistance R and the effective thermal resistance. From this it might be seen that the responsivity could be increased indefinitely by increasing the current. This is not possible in practice because there is an optimum temperature of efficient operation and so no further advantage is gained by increasing i beyond that necessary to reach that temperature.

General expressions for the responsivity and the time constant, τ, of a bolometer have been given as[17,18]

$$r = a\alpha v(G-\alpha_\omega)^{-1} \qquad 2.19$$

and $$\tau = C(G-\alpha_\omega)^{-1} \qquad 2.20$$

where

a = fraction of incident signal absorbed

α = temperature coefficient of resistance

C = thermal capacitance of bolometer

G = thermal conductance to bolometer heat sink

W = total power dissapated in bolometer

V = voltage applied to bolometer

For a bolometer to have maximum responsivity, α must be large with G small. However, if G is small relative to C the time constant will be long and so it is also necessary to keep C small. This can be done by reducing the weight and size of the element as much as possible. Cooling the bolometer reduces the thermal capacity and leads to large values of α[19] as well as reducing the noise level, hence improving the performance.

The minimum detectable power or noise equivalent power (n.e.p.) of a bolometer is defined[20] as the root-mean-square value of the sinusoidally modulated signal power required to produce an output voltage equal to the root-mean-square noise voltage. The n.e.p. of a thermal detector is given by[21]

$$\text{n.e.p.} = (16\sigma KT^5 A\Delta f/n)^{\frac{1}{2}} \text{ watts} \qquad 2.21$$

where

σ = the Stefan constant

K = the Boltzmann constant

A = detector area

Δf = amplifier bandwidth

n = fraction of photons absorbed

If A = 1 cm^2, Δf = 1 H_Z, T = 300K and assuming that the detector is an ideal black body for which n = 1, the n.e.p. is equal to 5.5×10^{-11} W. Often the term detectivity, D, is used instead of n.e.p. where

$$D = \frac{1}{\text{n.e.p.}} \qquad 2.22$$

In the case of the 'ideal' detector above $D = 1.8 \times 10^{10} W^{-1}$. From equations 2.21 and 2.22 it can be seen that cooling the 'ideal' bolometer leads to a very large increase in detectivity.

The bolometer used in this work is an antimony doped single crystal of germanium designed for operation at 1.5K. This temperature is reached by reducing the pressure in a liquid helium cryostat to $4.8 \times 10^{2} Nm^{-2}$. At 1.5K ($< 2.17K$) liquid helium is below its point for the HeI/HeII transition at which it becomes an anomalous superconducting liquid with zero viscosity. The superconduction makes HeII ideal for rapidly and smoothly cooling the bolometer and eliminating mechanical noise (due to bubbling).

The germanium has been doped with antimony so that absorption occurs at long wavelengths where germanium becomes transparent.

The antimony doped germanium bolometer is thought to operate both as a thermal and as a photoconductive detector. The antimony doping gives rise to donor levels close to the conduction band of the germanium. These are shallow levels due to n-type impurities and have ionisation energies in the order of 0.01 eV. Figure 2.4 shows a diagrammatic representation of this effect.

If we assume that the temperature T is such that $\Delta E_1 \gg KT$ then we can also assume that none of the donor levels are ionised and therefore will each contain one electron. Radiation falling on the detector will excite electrons into the conduction band if the condition $h\bar{\nu} > \Delta\epsilon$, is satisfied. This increase in the number of electrons in the conduction band is associated directly with a change of resistance of the bolometer element which is the detected signal. Operating in this mode germanium

Fig. 2.4 A Representation of shallow donor levels due to n-type impurities.

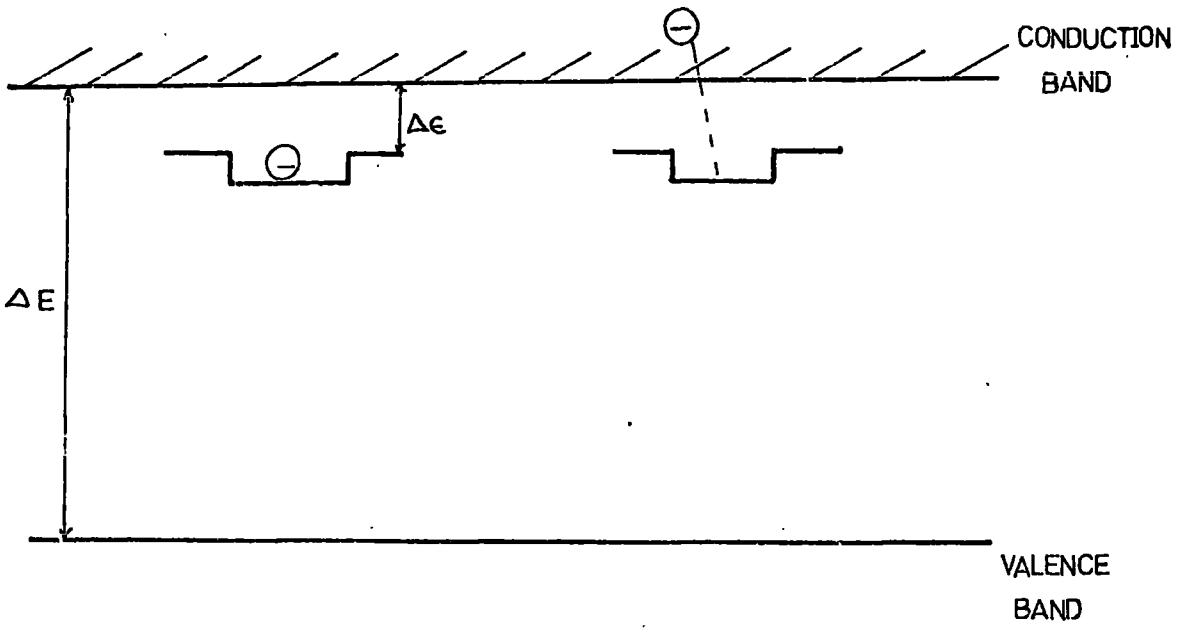

bolometers have very high speeds of response ($\sim 10^{-7}$s) and a low frequency limit[17] of about 75 cm^{-1}.

As a thermal detector the bolometer operates by excitation of electrons already in the conduction band. Thermal detectors generally have longer time constants but cover a wider frequency range than photo-conductive detectors. The doping of the germanium bolometer used in this work has been optimised to give increased absorption in the region 2 - 30 cm^{-1} and operates with a time constant of 0.8 ms at a noise level close to the Johnson noise limitation.[22] Because the mode of operation has not been fully established a calculated value of the theoretical responsivity

has little significance. However, it is possible to calculate the responsivity from the bolometer load curve[23] E vs I using equation 2.23

$$r = (Z-R)/2E \qquad 2.23$$

where

Z = dE/dI, the dynamic resistance.

Using the test circuit illustrated in figure 2.5 [22] the d.c. load curve for the bolometer element at 1.5K has been obtained and is shown in figure 2.6. R_L is the load line calculated for the bolometer operating with a 8.1v bias and a load resistance of $1M\Omega$. From this the operating voltage E = 3.5v and the current passing I = 8.1μA have been determined. Figure 2.7 shows a plot of LogI against LogR which has been used to obtain the resistance R of the bolometer with a current I passing. With a current of 8.1μA passing the resistance R = $575K\Omega$. By substitution of these values into equation 2.23 the responsivity of the bolometer at 1.5K is given as $7.6634 \times 10^4 VW^{-1}$.

R_L' shows a theoretical load line for the bolometer operating at 1.5K with a $1.5M\Omega$ load resistance. In this case the operating conditions are E = 3.25V, R = $724K\Omega$ and I = 5.4μA. The theoretical responsivity of the bolometer under these conditions is $9.1452 \times 10^4 VW^{-1}$ which is slightly greater than the calculated value for a $1M\Omega$ load resistance and therefore it may be advantageous to operate the bolometer with a $1.5M\Omega$ load resistance.

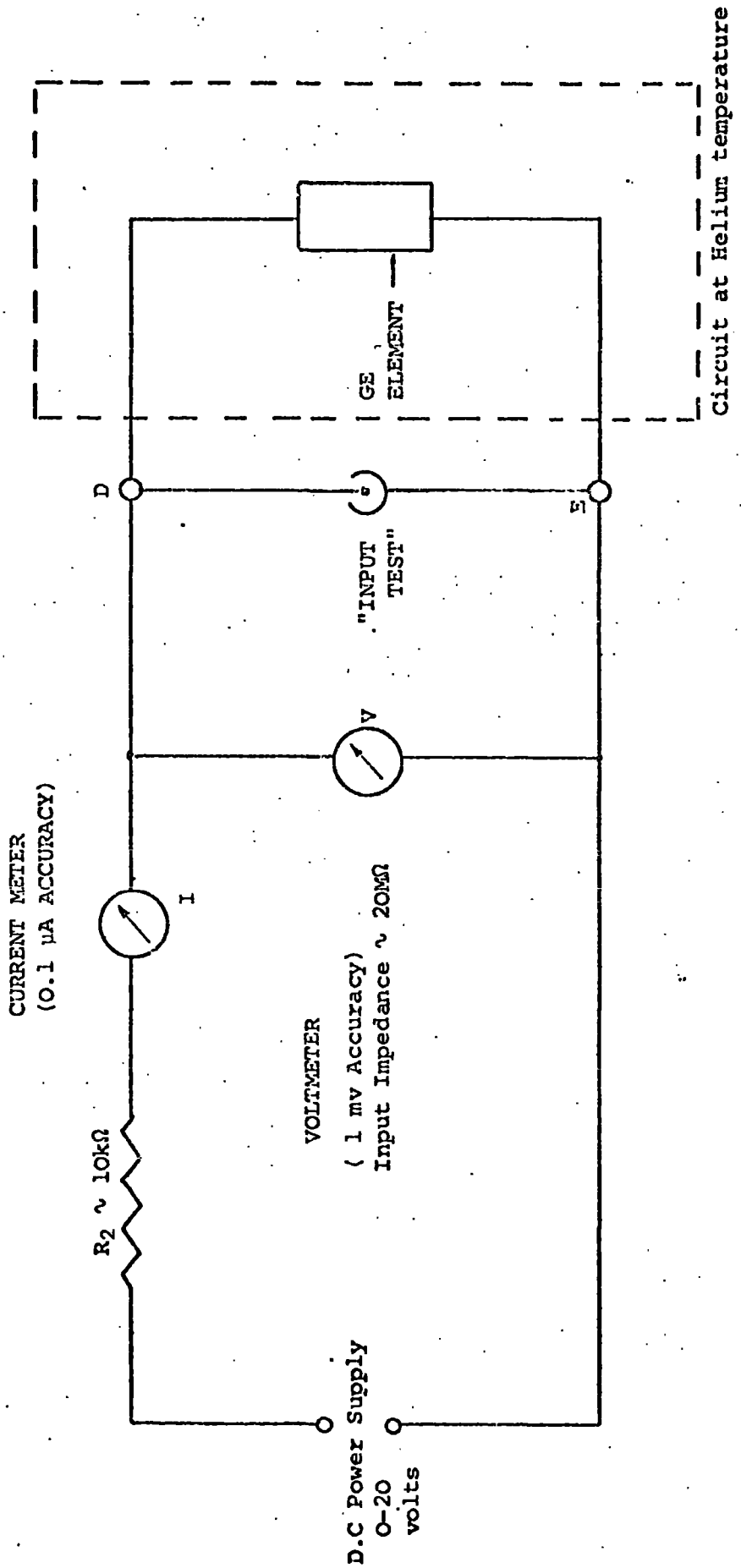

Fig. 2.5 The d.c. load test circuit for the bolometer

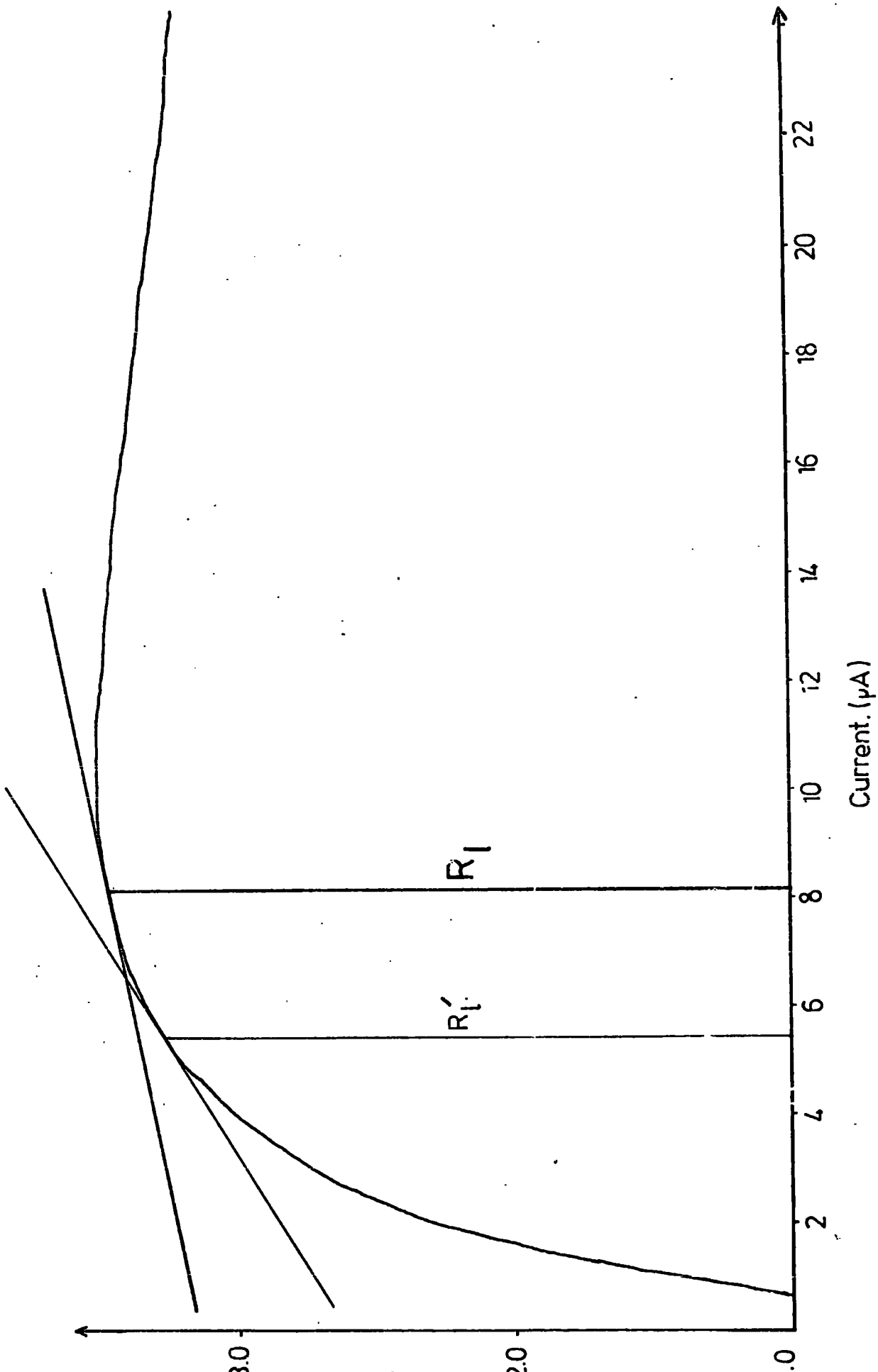

Fig. 2.6 d.c. load curve for the bolometer

Fig. 2.7 Graph of log I vs Log R for the bolometer

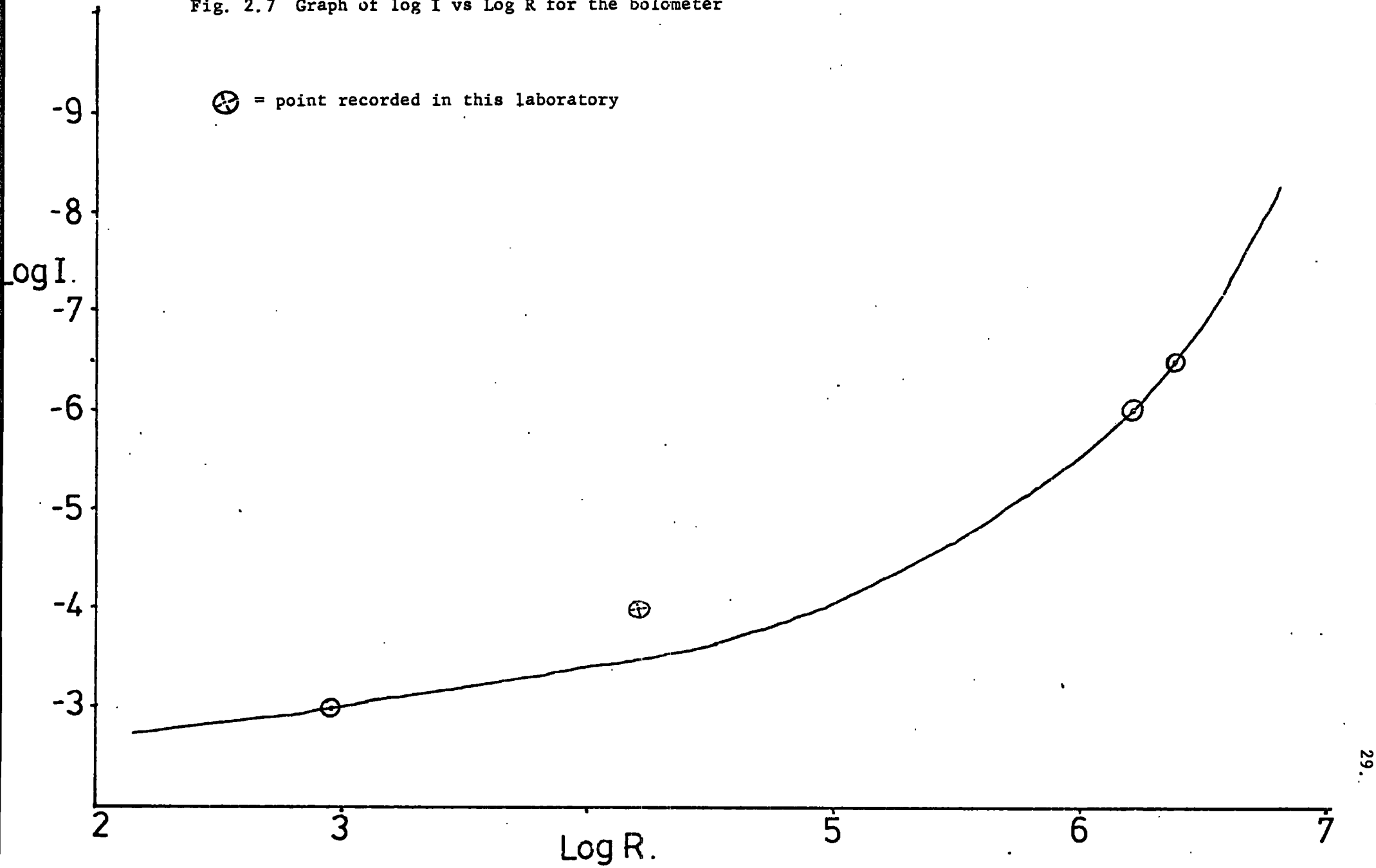

Advantages of the bolometer described over other detectors

A great deal of the 'current noise' arising from multicrystal semiconducting bolometers is believed to be generated at the many crystal junctions of the element.[17] By using a single crystal this source of noise is eliminated and therefore the bolometer described should have some advantage in noise level over a multicrystal detector such as the carbon flake bolometer.

The bolometer has advantages over the standard golay detector in signal to noise ratio, speed of response and low frequency cut off. However, the upper frequency (short wave length) limit of the golay is typically much higher than the bolometer used in this work. Some comparisons of detector performances are shown in table 2.1.[19]

Table 2.1 A comparison of some far infrared detectors

etector	Temp(K)	n.e.p (at 1 Hz)	Response time(sec)	Low frequency Limit	High frequency Limit
deal thermal olometer	1.5	10^{-16}-10^{-17}	-	-	-
deal photocond-ctive bolometer	1.5	10^{-13}-10^{-14}	$\phi 10^{-7}$	-	-
olay cell	300	10^{-10}	10^{-2}	$*_{20cm^{-1}}$	$*_{5000cm^{-1}}$
arbon bolometer	2.1	3×10^{-11}	10^{-3}	whole sub mm band	-
ermanium olometer	2.1	3×10^{-12}	$\dagger *_{8x10^{-4}}$	$*_{2cm^{-1}}$	$*_{\sim 200\ cm^{-1}}$

* values for system used in this work

† at 1.5K

ø ref. 17 p.167

ii) The polarising system

In the conventional interferometer the beamsplitter gives maximum efficiency when it is 50% transmitting and 50% reflecting. Under these ideal conditions a total of 50% of the source radiation will recombine and pass through to the detector while the other 50% is reflected back to the source. If the reflectivity is greater than, or less than the transmitivity the total radiation reaching the detector will be less than 50% since each beam undergoes one reflection and one transmission. The second problem encountered with thin film beam splitters is that their efficiency is frequency dependent. Because of this they have an efficiency pattern as shown in figure 1.4. This means that at certain frequencies a very low signal is likely and so it is necessary to change beamsplitters and try to match up spectra in order to cover a broad frequency range.

The third problem encountered with 'conventional' instruments is that they give the interferogram modulation about a mean level. This means that there is a large component, the stability of which is dependent on the system (the electronics etc.). This has to be subtracted from the interference function before the interferogram, I(x) can be Fourier transformed (see Chapter Ic) and errors are likely to be introduced due to instrument variations.

These problems can be overcome by the use of the polarising interferometric system developed by Martin and Puplett.[1] In this system the beamsplitter is constructed from many free standing parallel wires mounted in a rigid frame. Wire grids manufactured in this way reflect

radiation with its plane of polarisation parallel to the plane of the wires and transmit radiation with its plane of polarisation normal to the plane of the wires (see figure 2.8).

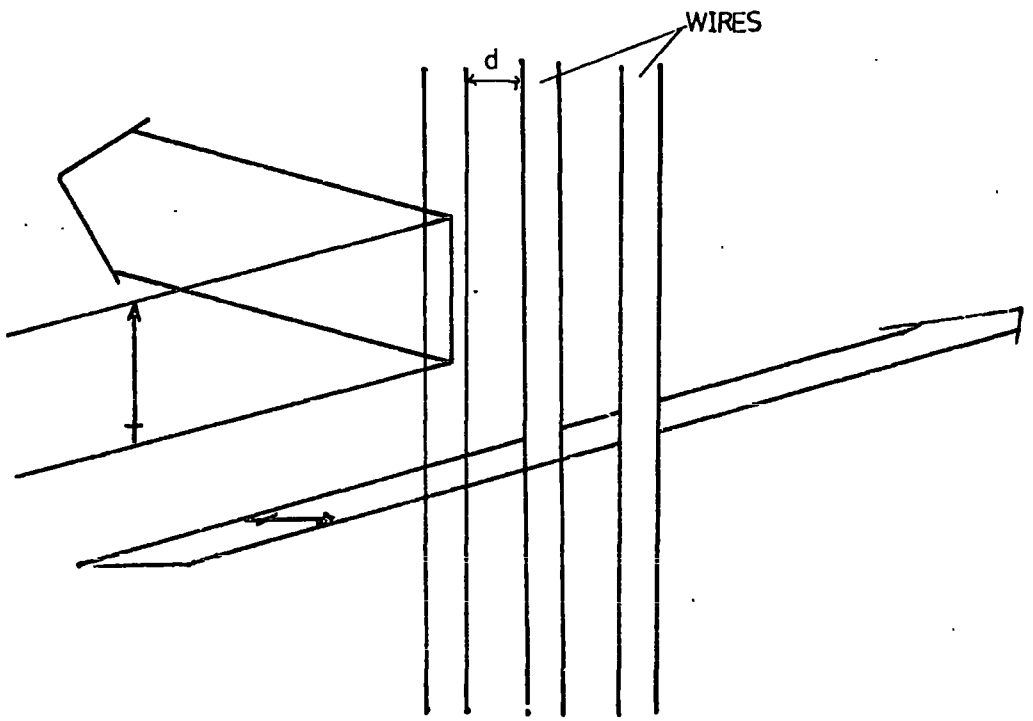

Fig. 2.8 Reflection and Transmission of light at a wire grid.

The efficiency of these grids is almost 100% for the appropriate plane of polarisation up to the frequency limit given by equation 2.24.

$$\bar{\nu}_{max} = \frac{1}{2d} \qquad 2.24$$

where

d = the spacing between the wires.

The complete polarising system is illustrated by figure 2.9. The radiation beam is first polarised by P_1 at 45^o to the page. The beam is then divided by the wire grid beam splitter which has its plane of polarisation normal to the page. Half of the beam is polarised normal to the page and reflected onto m_2 whilst the other half is polarised parallel to the page and is transmitted onto m_1. The mirrors m_1 and m_2 are retroreflectors as shown in figure 2.10. When the beams of polarised radiation are reflected by the retroreflectors their electric vectors are rotated by 90^o as shown in figures 2.11 and 2.12. After reflection beam 1 will be polarised normal to the page and will therefore be reflected when striking the wire grid beam divider D for the second time. Similarly beam 2 undergoes a 90^o rotation of its electric vector on reflection from m_2 and is transmitted when striking D for the second time. (Note that in this system none of the radiation has been reflected back to the source). Finally the recombined beam is plane polarised by P_2 and has amplitude which varies with path difference as in a conventional interferometer. The analyser P_2 can have its axis either parallel or perpendicular to P_1 which gives equations 2.25 and 2.26 for the intensity.

$$I_{\parallel}(x) = \frac{I_o}{2}(1 + \cos 2\pi\bar{\nu}x) \qquad 2.25$$

$$I_{\perp}(x) = \frac{I_o}{2}(1 - \cos 2\pi\bar{\nu}x) \qquad 2.26$$

where

$I_{\parallel}(x)$ is for P_1 parallel to P_2.

and

$I_{\perp}(x)$ is for P_1 perpendicular to P_2

The two interferograms obtained for P_1 and P_2 parallel and perpendicular are 180^o out of phase. By rotating P_1 it is possible to alternate between

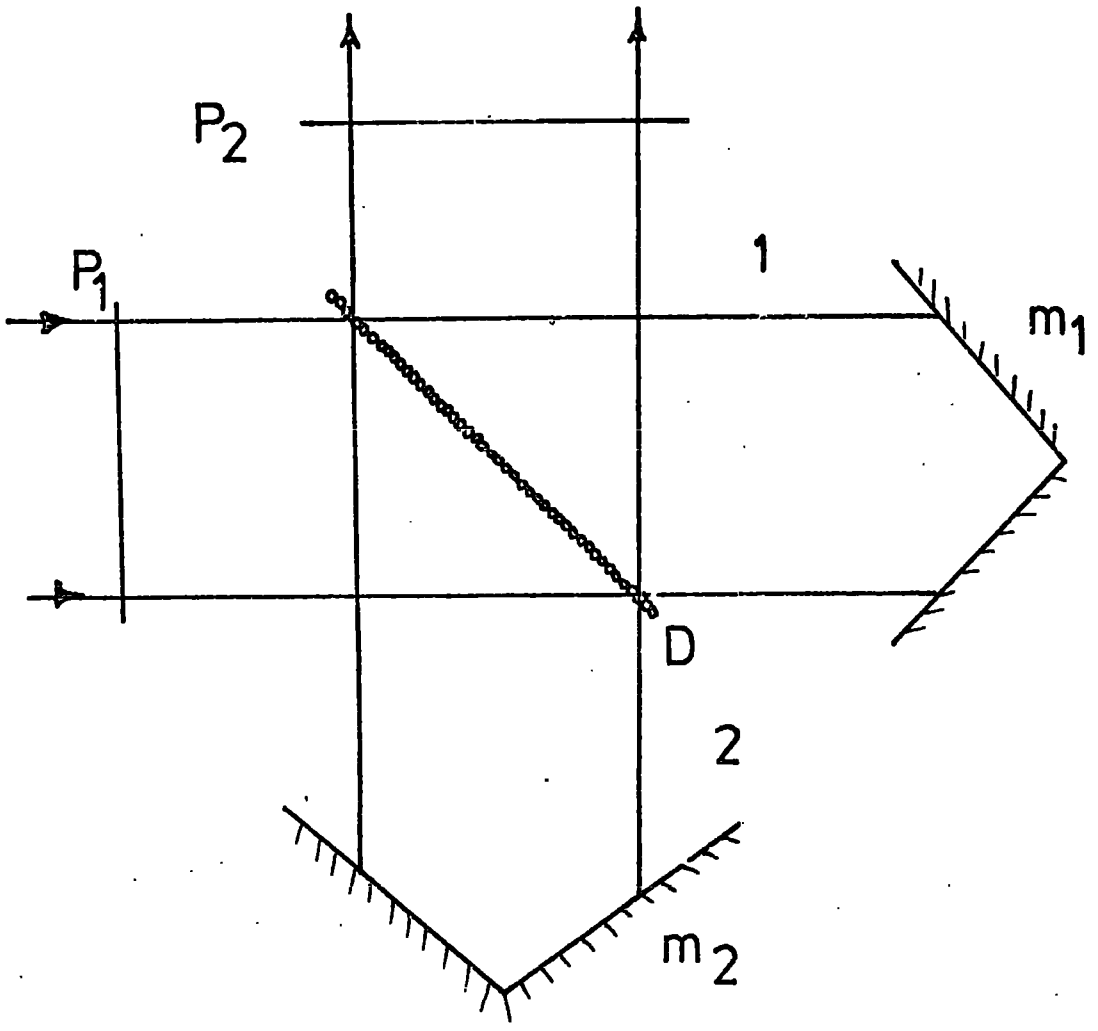

Fig. 2.9 Optical configuration of the polarising interferometer system

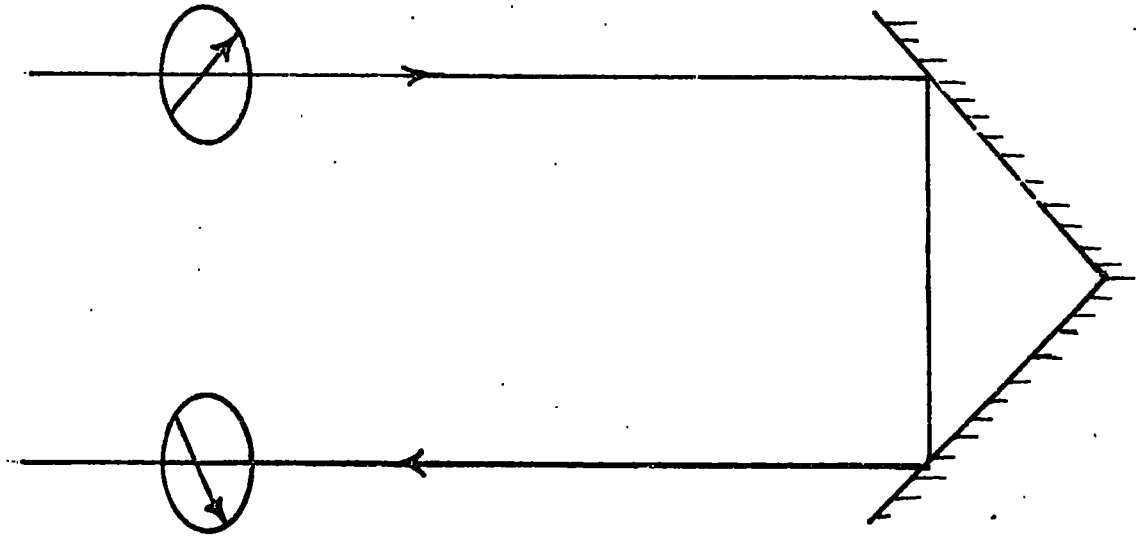

Fig. 2.12 Diagram illustrating the rotation of the electric vector of a radiation beam at a retroreflector

Fig. 2.10 A retroreflector used in the polarising system

Fig. 2.11 Photograph showing rotation of image at a retroreflector

these two conditions instead of chopping the signal in the conventional way. This method gives an interferogram which oscillates about a true zero mean-level. Equations 2.25 and 2.26 can then be replaced by equation 2.27

$$I_{\parallel}(x) - I_{\perp}(x) = I_o \cos 2\pi\bar{\nu}x \qquad 2.27$$

The polarising system used in this work was manufactured by Queen Mary College Industrial Research Ltd., London. The tungsten wire-grids were wound with a spacing of 3.33×10^{-3}cm over a standard beam-splitter ring and a specially manufactured chopper ring (P_1). The spacing of the wires gives the theoretical maximum frequency limit of 150 cm^{-1} from equation 2.24. The analyser was a photolithographically prepared mylar grid mounted in the sample compartment immediately before the sample.

Due to the lack of a dc component in the interferogram it was necessary to include a 3V offset on the FS 200 electronics to ensure that only positive signals reach the A/D system. Another problem was encountered due to non-linearity of the electronics when receiving the large signals associated with this optical system. This and other problems are discussed fully in section 2c.

(b) The Practical operation of the system

(i) The Bolometer

The bolometer, as described in Chapter 2a is mounted on a copper block at the base of an Oxford Instruments Ltd. MD800 cryostat (Figure 2.13). This cryostat consists of two cans, one of 1.4 litre capacity which is the reservoir for the liquid helium, and one of 1.7 litre capacity which holds liquid nitrogen to provide a radiation shield for the helium. The entire outer case of the cryostat is evacuated down to about 1.3×10^{-2} Nm^{-2} using a two stage rotary oil pump in conjunction with a mercury diffusion pump. When the cryostat is filled with helium this vacuum jacket is further cryopumped down to about 1.3×10^{-4} Nm^{-2} and therefore provides very good thermal insulation. Initially, the vacuum jacket of the cryostat is pumped out for about 2 hours at room temperature to remove any volatile liquids such as water. In an effort to reduce the amount of liquid helium used in filling the cryostat both the nitrogen and the helium cans are precooled to 77K with liquid nitrogen. The nitrogen is left in the helium can for about an hour and then blown out with helium gas. The vacuum valve is then sealed off and the cryostat is ready for filling with helium.

The helium transfer is carried out using a standard Oxford Instruments transfer tube (with evacuated annular space) mounted in the seventeen litre bulk dewar as shown in figure 2.14. The transfer tube is gradually lowered into the bulk dewar so that a steady flow of helium gas begins to build up as the tube cools down. The flow rate is controlled by the football bladder, which is used to provide an overpressure, and the venting valve, which is used to vent off helium gas if the flow becomes too rapid. (This boil off of helium is minimised by lowering the transfer tube slowly). When cold helium gas is flowing from the

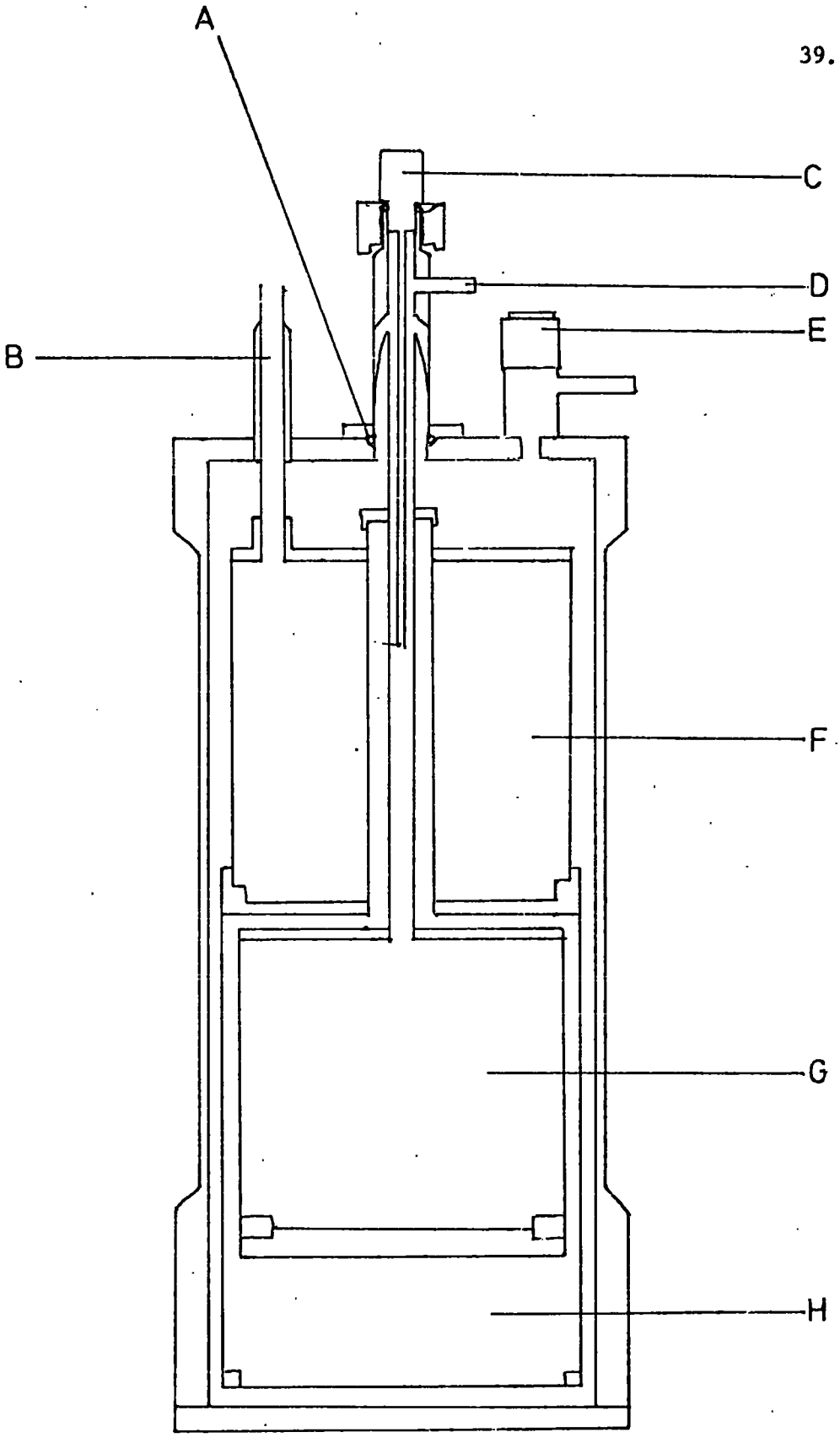

Fig. 2.13 Diagram showing cryostat construction

A = 'O' ring, B = nitrogen inlet, C = safety valve and helium inlet, D = helium pumping port, E = vacuum jacket valve, F = nitrogen can, G = helium can, H = bolometer chamber

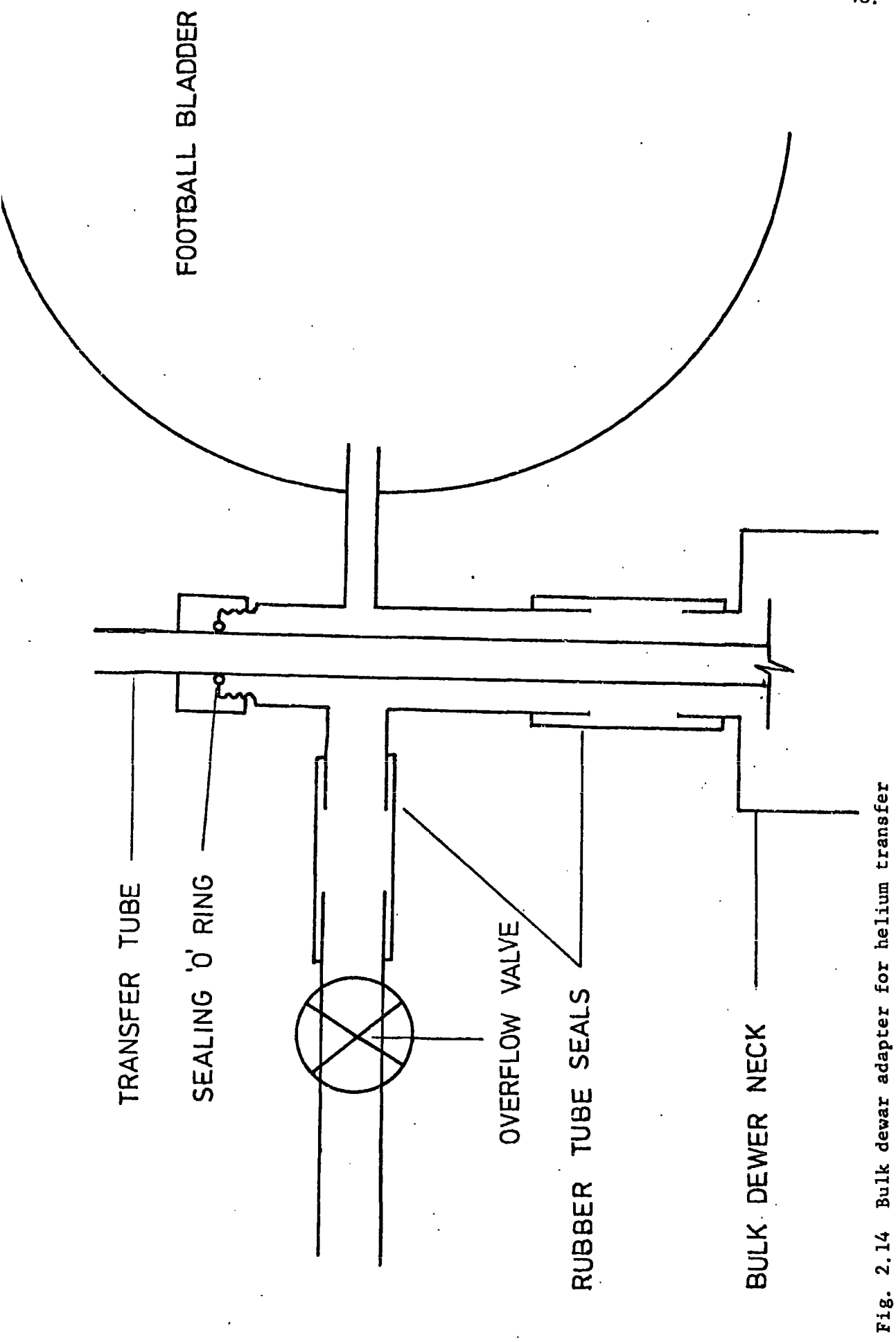

Fig. 2.14 Bulk dewar adapter for helium transfer

transfer tube the bulk dewar is raised on a lift to enable the free end of the tube to be inserted into the cryostat neck. The lift is then lowered so as the two ends of the transfer tube are about $\frac{1}{2}$ to 1" from the bottom of the cryostat and dewar. Initially the flow rate, which is observed by the plume of gaseous helium at the cryostat neck, is quite fast as the liquid helium is boiled off very rapidly by the relatively warm helium can. After about 10-15 minutes the cryostat has cooled down to liquid helium temperature and begins to fill. This is observed by the drop in venting rate of gas and a few initial oscillations of flow. The cryostat then takes about 5 minutes to fill with the required 1.4ℓ of liquid helium. When the cryostat is full a 'bluish' plume of helium liquid can be seen at the cryostat pumping port. Throughout the filling process it was necessary to play a warm air dryer over the top of the cryostat to prevent the sealing 'O' ring A from freezing which would result in a loss of vacuum in the outer case.

The full cryostat is now connected up to a double stage 330L/min rotary oil pump to reduce the pressure in helium can and therefore lower the bolometer to its working temperature of 1.5K. The pump down procedure is done slowly to conserve the helium as much as possible and usually it takes an hour for the pressure over the helium to reach 35 torr, the λ point for the HeI, HeII transition. Below this pressure (corresponding to 2.17K) the main pumping valve is opened fully and the cryostat then takes a further half an hour to reach 1.5K. Throughout the pump down procedure it is necessary to continue warming the cryostat neck to prevent the 'O' ring from freezing. To reverse the process and bring the cryostat up to atmospheric pressure (for refilling) it was important that the helium can was vented with dry helium gas to avoid the possibility of any condensation in the neck which might cause a blockage.

The detector is fitted onto the interferometer with a short adjustable light guide as shown in figure 2.15.

Fig. 2.15 Cooled detector light guide attachment.

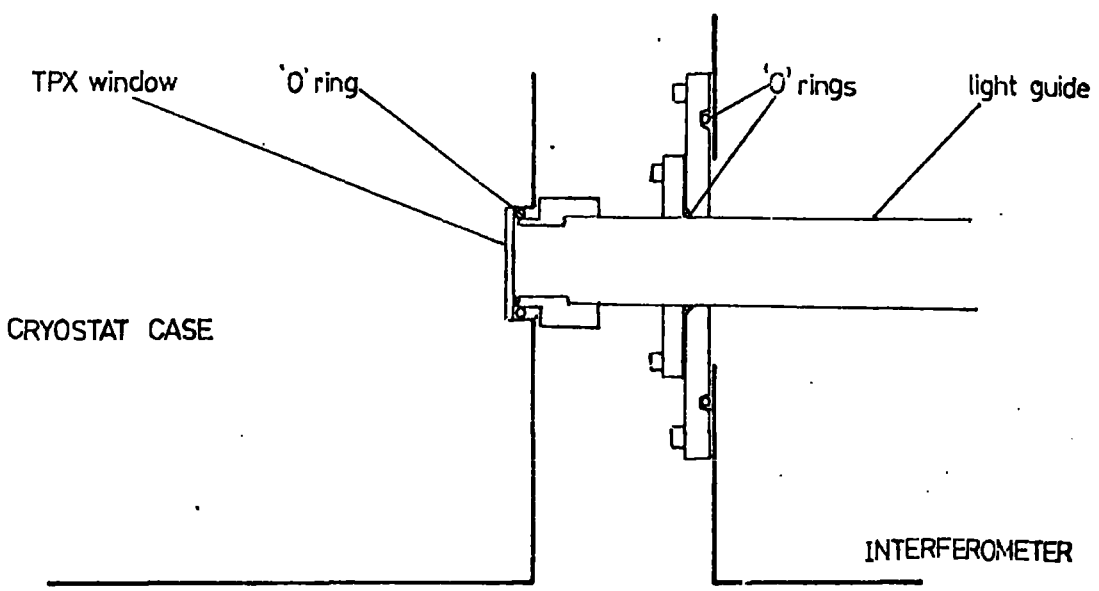

With the mirrors set at the point of zero path difference the signal from the detector is maximised by sliding the tight guide in slowly. It was found that this was the only additional optical alignment necessary when using this detector as the angle subtended to the instrument was not critical. Figure 2.16 shows the detector in the working configuration. All other optical alignments were carried out as normal, but with the source stopped down to 3 mm to avoid overheating the bolometer element with excess radiation.

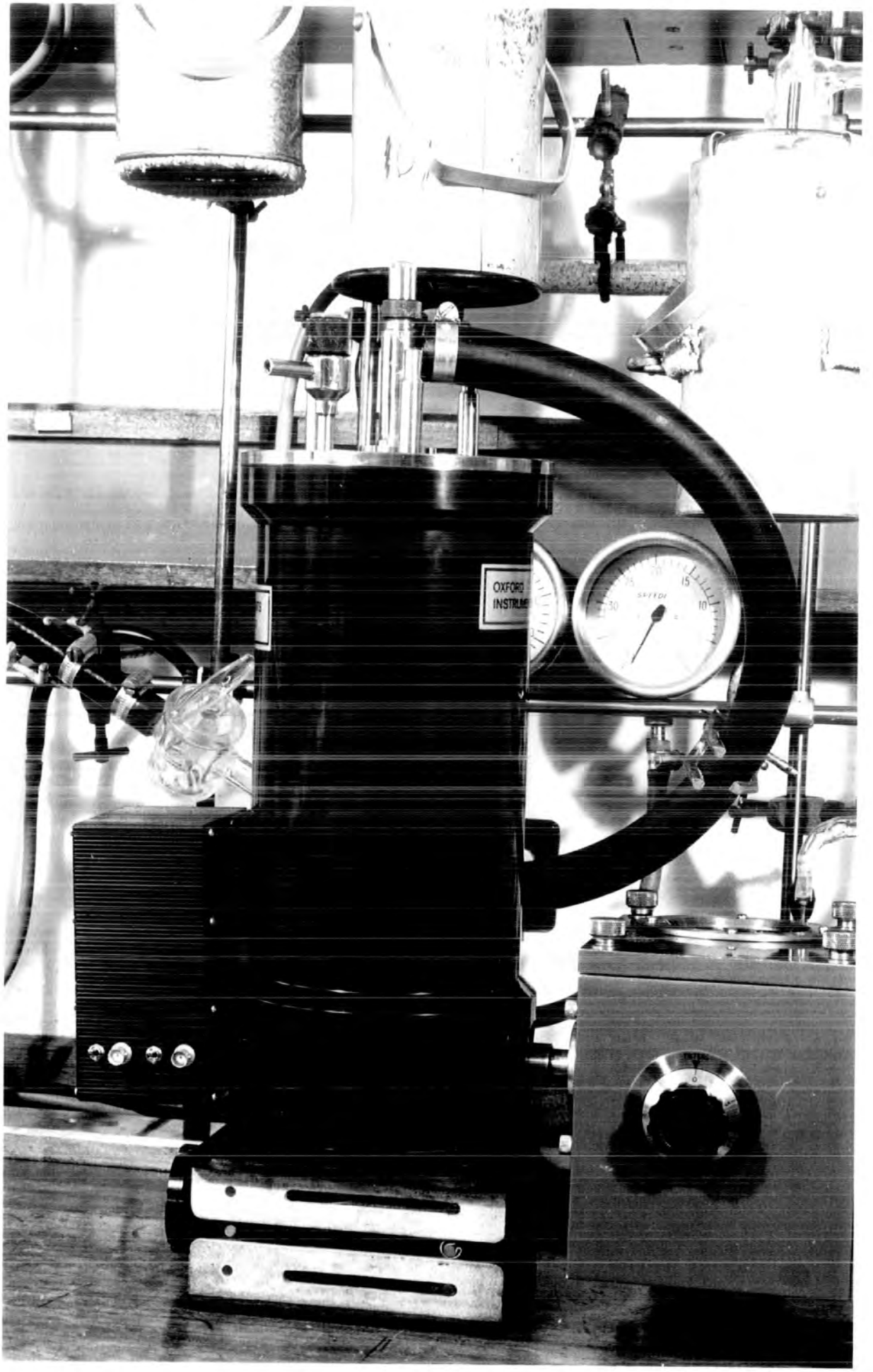

Fig. 2.16 The cooled detector in the operating configuration

It was necessary to adjust the phase reference signal from the chopper when using the cooled detector and this was done in the normal way with an oscilloscope connected to the 'ref' position on the R11C FS 200 electronics module. Due to the inherent time constants on the bolometer preamps three gain settings, 40dB, 50dB, 60dB, a slight phase adjustment was also needed if the usual 50dB gain setting was altered. Failure to rephase on alteration of the gain setting does not cause any distortion of the signal but does decrease the maximum amplitude of modulation.

At 1.5K the cryostat has a hold time of at least 24 hours providing that the liquid nitrogen can is topped up every 8-12 hours. At 4.2K with the radiation port closed the cryostat will hold for about 70 hours with the liquid nitrogen level maintained.

The resistance of the bolometer element at 4.2K was 3.21KΩ and at 1.5K increased to approximately 15.1KΩ. These readings were taken using a digital 'Fluke' meter set on the 20KΩ range and therefore passing a current of approximately 100μA. (Because the bolometer element is a semiconductor the resistance measured is dependent on the current injected).

The power to the bolometer preamp is provided by two 12.6V and one 8.1V mercury batteries. A further 8.1V mercury battery provides a bias voltage for the bolometer element. These batteries were checked frequently and a typical set of voltage readings is given in table 2.2.

Table 2.2 Voltages of detector supplies

Battery	Voltage off load	Voltage on load
Preamp	12.6v	11.7v
Preamp	12.6v	11.7v
Preamp	8.1v	7.9v
Bias	8.1v	8.0v

(ii) The polarising system

When setting the instrument up in the polarising mode the two plane mirrors are replaced by retroreflectors. The fixed retroreflector is secured with three allen screws in the same way as the standard mirror. The plane mirror on the moving arm of the interferometer is mounted on rubber pads. These have to be cut away to remove the mirror but they can be easily replaced with 1mm rubber gasket material when the instrument is being set up in the conventional mode. The retroreflector is mounted on the moving arm of the interferometer with a single central screw about which it can be easily rotated for alignment. Due to the optical configuration of the system it is necessary to include a 5cm aluminium spacer between the moving mirror arm and the interferometer body in order to keep to point of zero path difference approximately in the centre of the drive travel. The spacer used brings the point of zero path difference to about 900 on the drive scale the centre of which is at 1000.

The initial alignments of the polarising interferometer are done with the chopper unit removed and with a mylar beam splitter in place. The mirror in the fixed arm of the interferometer is rotated so that the images of the source cross wires are parallel when viewed with the inspection mirror. This alignment must also be checked by viewing the images of the roofs of the two retroreflectors which must appear to be parallel (in the plane of the bench) and not displaced from each other by more than 1mm. When attempts are made to align the retroreflectors in the vertical plane the cantilever adjusters have very little effect because of the optical configuration of a retroreflector mounted in this way. Therefore alignment in the vertical plane is achieved by tilting the beam-splitter frame after loosening the supporting gimbals.[25] The

mylar beam-splitter is then replaced by the wire-grid beam-splitter which is viewed with the inspection mirror. The wire grid is rotated in the beam-splitter holder to such a position that the image of the grid wires is perpendicular to the wires viewed directly. This position was then marked on the beam-splitter and holder for future reference. The polarising analyser and modulator were then installed and the source switched on. With the offset voltage set on the amplifier to ensure that only positive signals were recorded the moving retroreflector was moved to a point some distance away from zero path-difference where the signal should be small. The signal was observed on an oscilloscope connected onto the 'amp' monitor point on the RIIC FS200 electronics. The analyser was then rotated until the minimum signal was observed (without an offset voltage this signal should be zero).

The phase setting of the system was done in the usual way, that is by rotation of the phase triggering photoswitch about the modulator ring whilst using an oscilloscope to monitor the output from the 'ref' position on the FS200 electronics. However, using this system it is necessary to make the phase adjustment on the point of zeropath-difference. This is due to the positive and negative phase changes which occur when passing through the ZPD with a polarising interferometer. Final adjustments were made to mirror alignment and analyser orientation to achieve the maximum signal at zero path difference.

The operation of the interferometer in the polarising configuration was the same as the standard instrument except for the offset voltage of up to 3v which had to be applied to maintain a positive signal in the amplifier. Due to the greater throughput of the system it was often necessary to use a smaller source apature than normal to avoid over-heating the detector. This problem was particularly apparent when

using the bolometer which, when overheated, records interferograms of the form illustrated by figure 2.17.

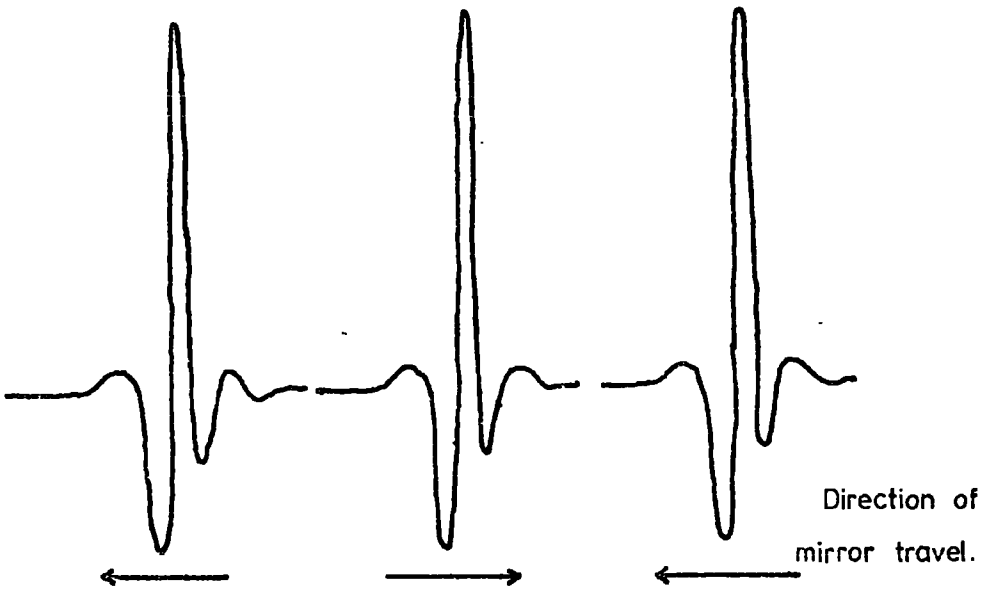

Fig. 2.17 The shape of the interferogram recorded when the bolometer is overheated by the incident radiation.

(c) Results

(i) The polarising system

Initially, the spectra recorded using the polarising system showed some distortion in both the high and low frequency regions. In the low frequency region there was a feature at approximately 10-8 cm^{-1}, whilst the high frequency cut off was much lower than the theoretical limit of 150 cm^{-1}. Figures 2.18 and 2.19 show the 8 cm^{-1} feature and the high frequency cut off at approximately 110 cm^{-1}. The interferograms associated with the distorted spectra had disproportionatly large negative lobes near the point of zero path difference. The ratio of the depth of the negative lobes to the full height at maximum modulation was 38% instead of the expected[24] ratio of 25%. It was found that the distortion did not occur when the amplifier was replaced by a Brookdeal 9401. Therefore the distortion was thought to arise from electrical non-linearity due to overloading of the FS200 amplifier. The following modification to the electronics were then carried out.

The diode MR1[26] was shorted out of the circuit and the resistors R24 and R25 were changed from 10KΩ to 47KΩ and 4.2KΩ respectively.

The spectra recorded with the modified electronics no longer showed a low frequency feature but the high frequency cut off was still very low. Figure 2.20 shows a spectrum recorded with the modified FS200. The high frequency cut off is about 110 cm^{-1}. Extensive optical alignment of the instrument gave no significant increase in frequency range when the data was computed at Durham with FTRAN5. However, identical data sets computed at Queen Mary College Physics Department showed that the performance was more satisfactory. For example, figure 2.21 shows a spectrum computed at Queen Mary College with a high frequency limit

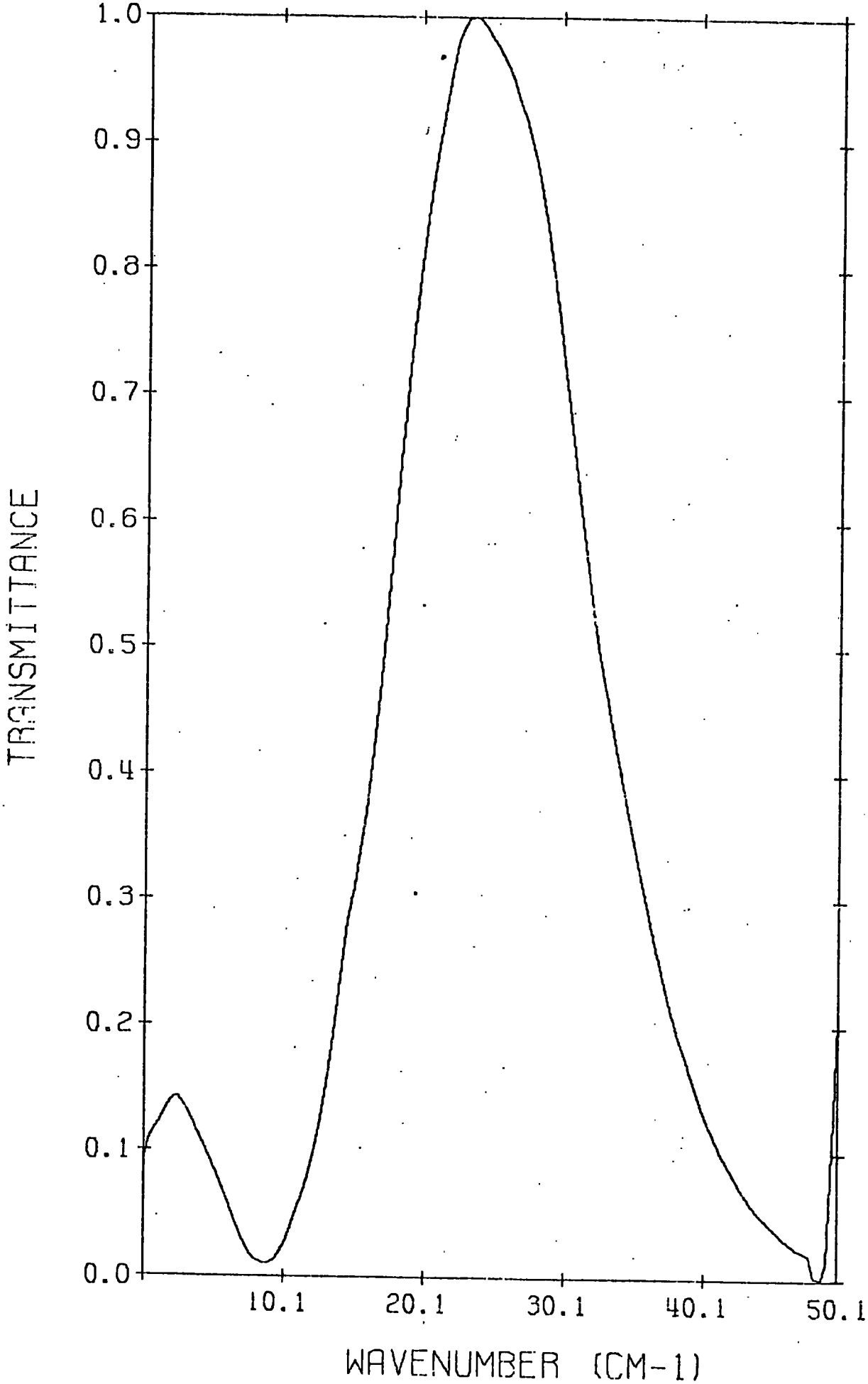

Fig. 2.18 Background spectrum recorded with the polarisers and the cooled detector (3mm black polythene filter)

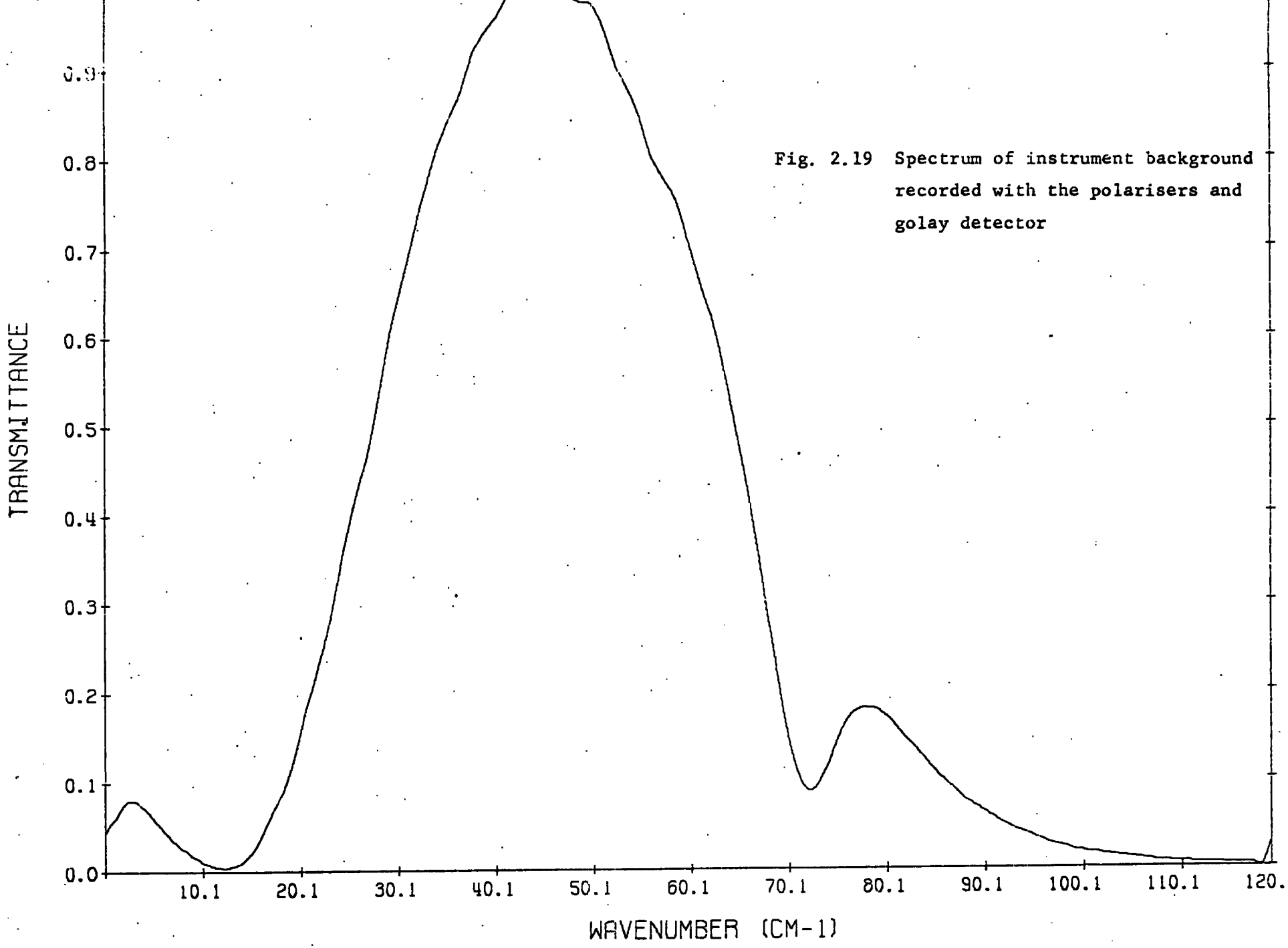

Fig. 2.19 Spectrum of instrument background recorded with the polarisers and golay detector

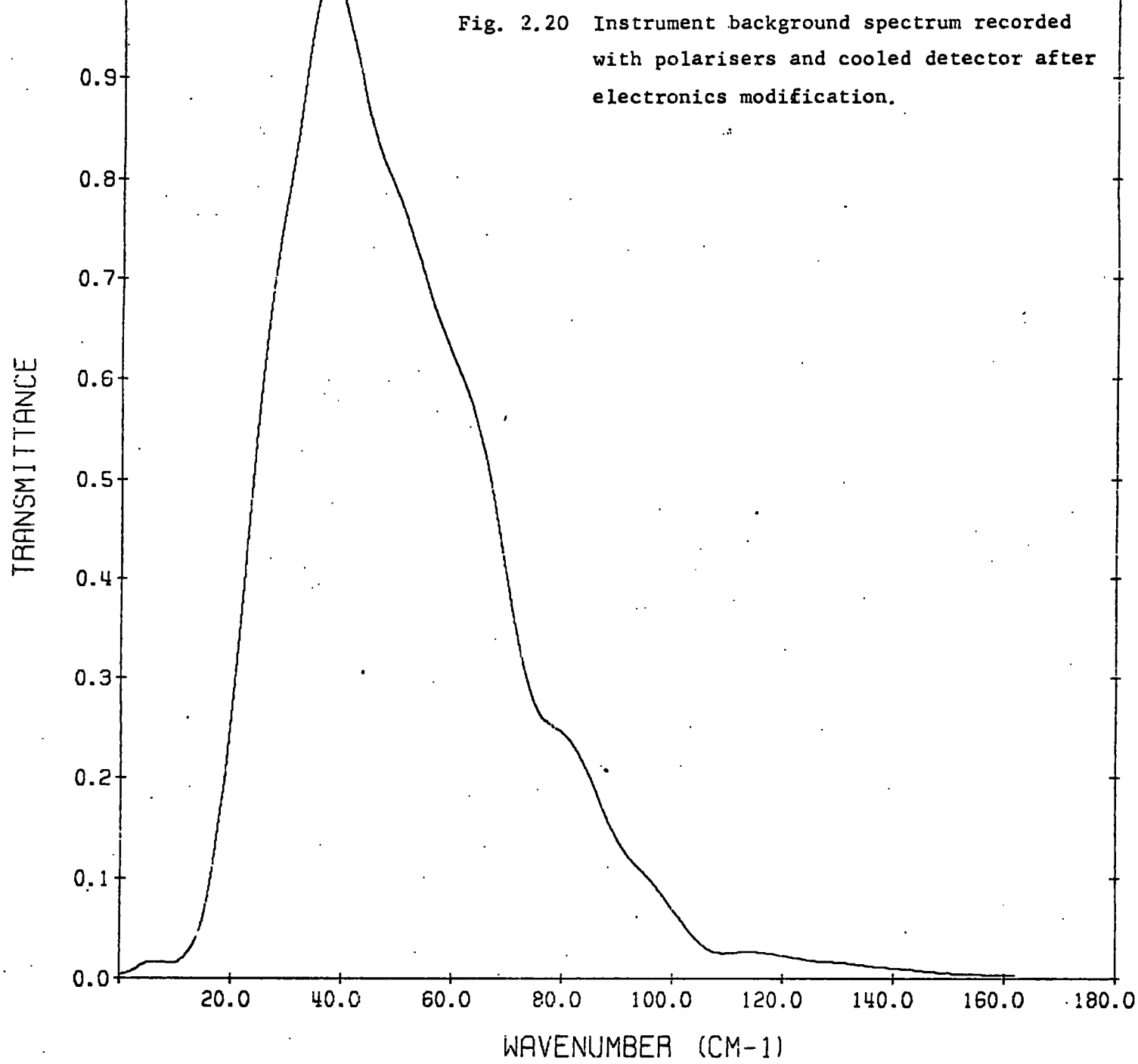

Fig. 2.20 Instrument background spectrum recorded with polarisers and cooled detector after electronics modification.

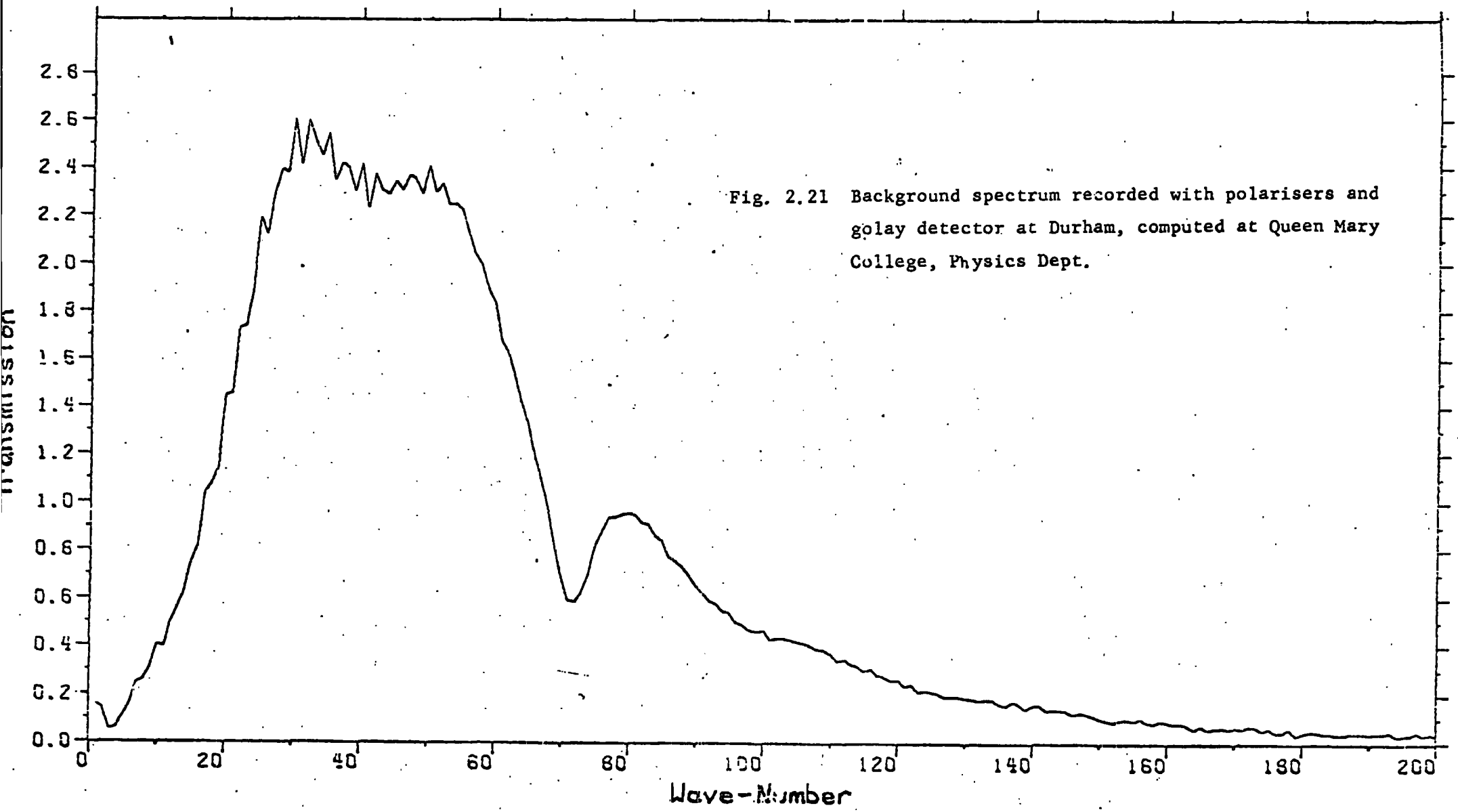

Fig. 2.21 Background spectrum recorded with polarisers and golay detector at Durham, computed at Queen Mary College, Physics Dept.

of 200 cm^{-1} and approximately 5% transmission at 150 cm^{-1}. At present it is thought that this software problem may arise from the mean level I_o subtraction which is performed on the interferogram before Fourier transformation. In the program FTRAN5 the magnitude of the mean-level I_o is taken to be the average of the entire interferogram and for the conventional interferometer this has been comparable with the interferogram level in the 'wings' (the true value of I_o). However, with the polarising system, in which the mean level is imposed by the d.c. offset, the average of the entire interferogram has been found to be up to 10% different from the true value of I_o taken from the 'wings' of the interferogram.

Investigations are currently being carried out into the effects on high frequency attenuation when different values of I_o are computed in the program.

(ii) The cooled detector

The static signal to noise ratio tests carried out on the bolometer were not satisfactory or indicative of the real performance in operation. It appeared that the detector was noisier when the radiation was blocked off than with radiation falling on it. This is believed to be due to the overheating of the element by the hot source and surroundings. The unfavourable temperature of operation leads to a loss of sensitivity and hence a drop in noise level. With the radiation blocked off the bolometer element reaches its optimum operating temperature of 1.5K and becomes more sensitive. Therefore the noise level is much higher. However, the signal/noise ratio should be the same or better because the increased sensitivity will also lead to an increase in signal intensity. An attempt is being made to prevent the bolometer from being overheated

by including an adjustable iris between the sample and the detector to decrease the radiation intensity when the sample is not strongly absorbing in the far infra-red.

Figure 2.22 shows a low resolution (2.44 cm^{-1}) water vapour spectra recorded with the bolometer. The drop in energy at low frequency in this case is due to the beam splitter used and the lack of filtering. The background shape is not as good as expected with such a detector and it is thought that this may be due to the overheating effect mentioned above. However, figure 2.23 is a very good spectrum which was obtained by operating the bolometer with very heavy optical filtering. The spectrum shows the tail of a t.Butyl ammonium chloride band[30] recorded with a 400 gauge beam-splitter and a 3mm of black polythene (hence the 60 cm^{-1} cut off) filter through a 7.7mm pathlength of a 0.1M solution in benzene. This example shows good sensitivity and signal-to-noise ratio down to 5 cm^{-1} and seems to indicate that the bolometer was probably operating at its most efficient temperature.

Figure 2.24 shows the ratio spectrum of two thicknesses of tetra-bromoethane recorded using a 400 gauge beamsplitter and no filters. In addition to the strong bands at 64 cm^{-1}, 112 cm^{-1}, 146 cm^{-1} and 175 cm^{-1} (note that the 112 cm^{-1} and 175 cm^{-1} bands are not doublets but appear so because the strong absorption has lead to a ratioing of near zero intensity) there are small features at 10 cm^{-1}, 19 cm^{-1}, 30 cm^{-1} and 55 cm^{-1}. These features are clearly visible due to the extremely high signal-to-noise ratio which the bolometer has compared to other detectors operating at low frequency. This spectrum, and that shown in figure 2.22 also indicate a fall in detector sensitivity at around 200 cm^{-1}. This is due to the detector optical filtering which has been optimised for maximum low frequency response.

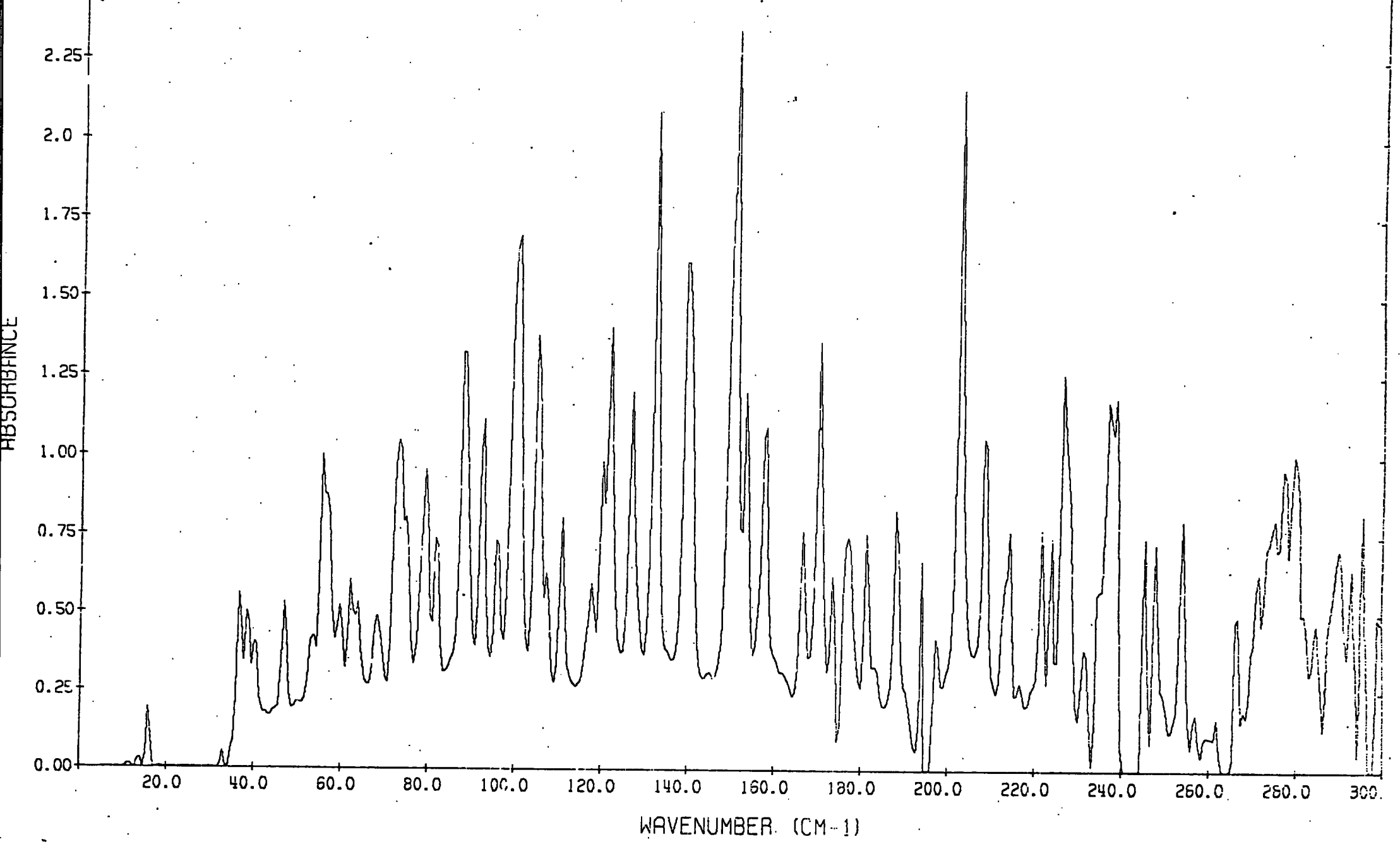

Fig. 2.22 Water vapour spectrum recorded with cooled detector

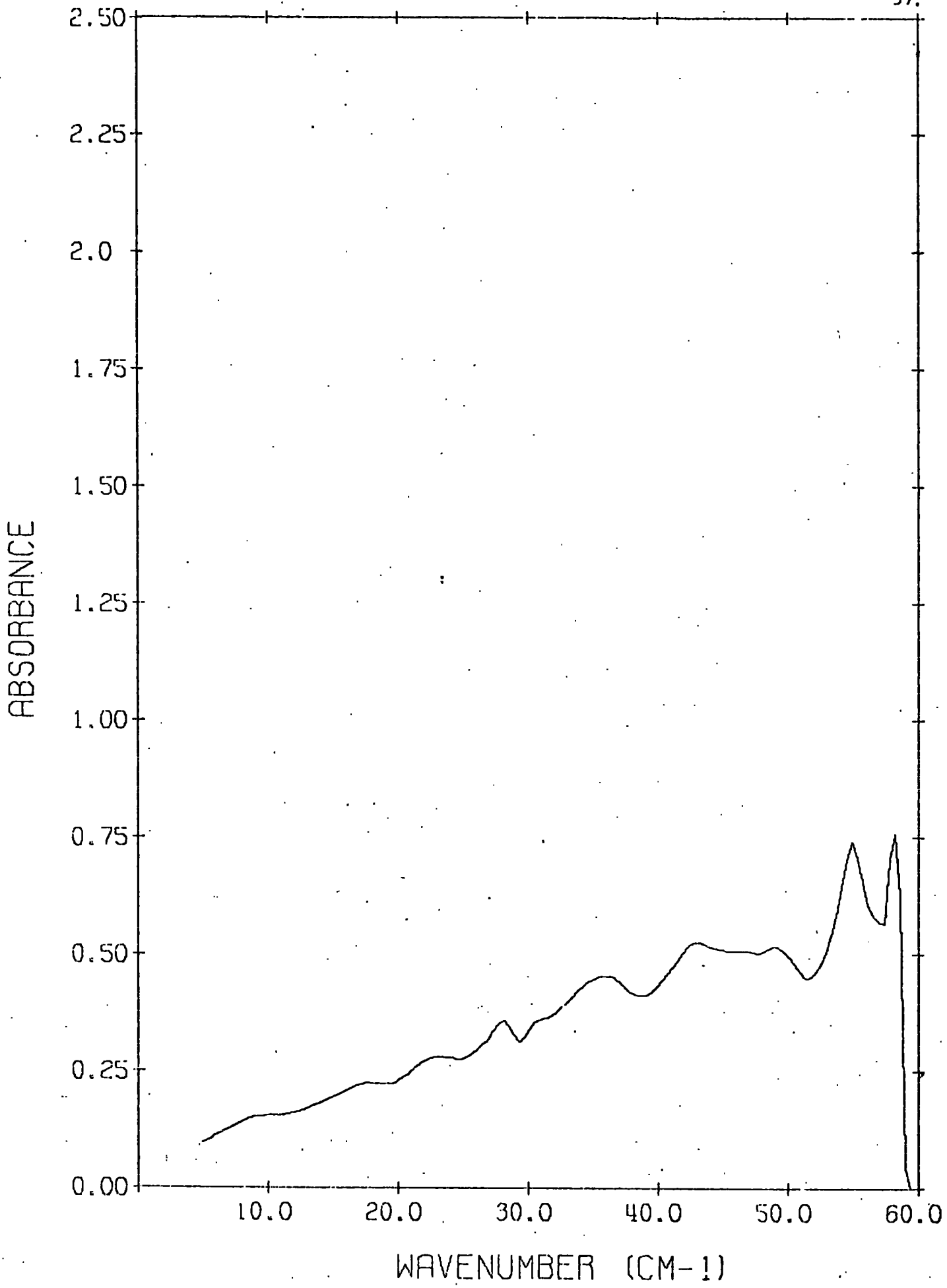

Fig. 2.23 Spectrum showing the tail of a t.butyl ammonium chloride band recorded with the cooled detector

Fig. 2.24 Spectrum of tetrabromoethane recorded with the cooled detector

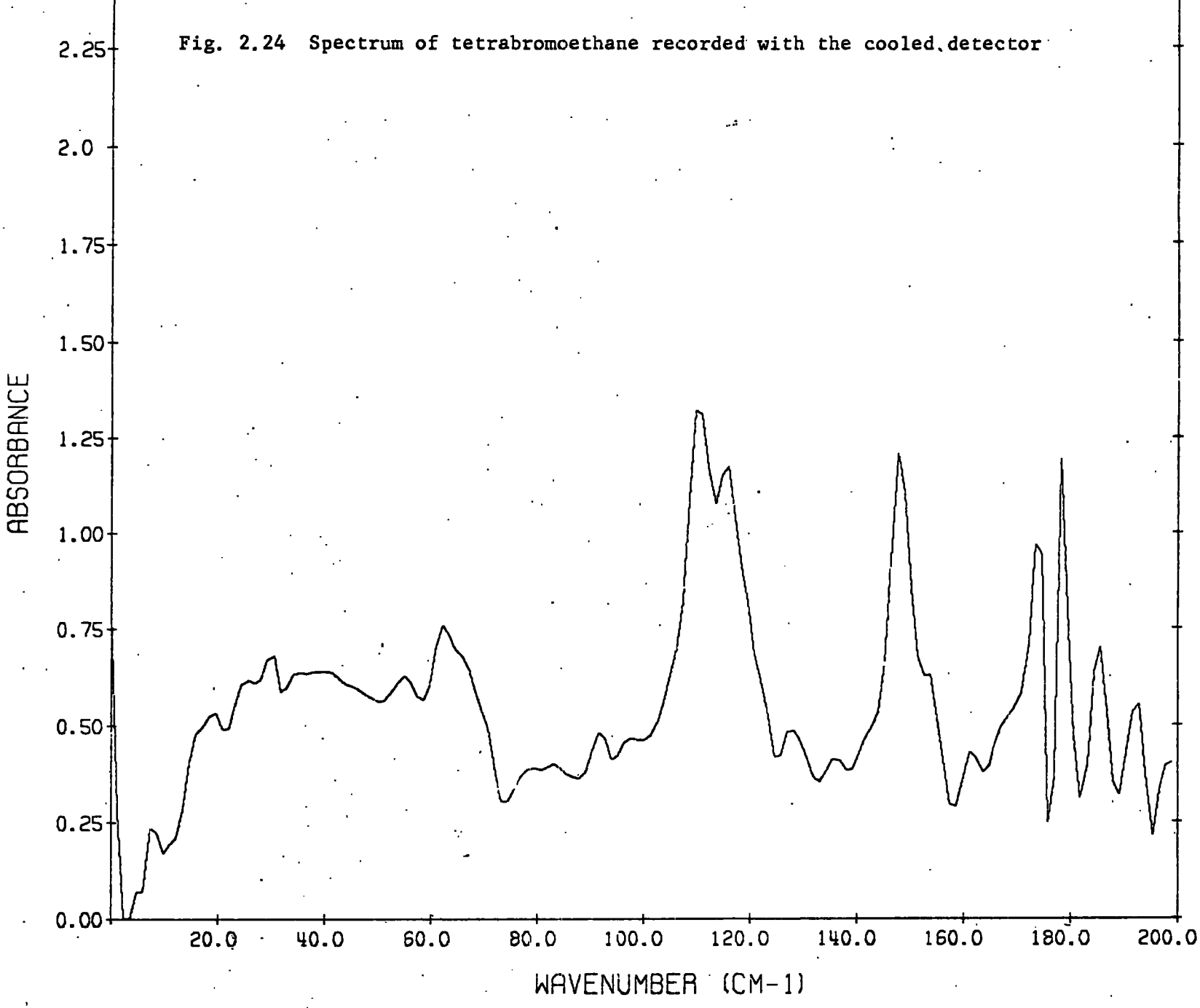

CHAPTER III

Development of the Refractive Index Module

a) Theoretical

In the physical, chemical and biochemical fields the far infra-red dispersion (refractive index) spectra can be used to compliment and elucidate the information obtained from the far infra-red absorption spectrum. For example, it has been shown[27] that the shape of the refractive index curve can indicate whether a spectral feature arises from a resonance or relaxation process (see Figure 3.1). In addition, the refractive index change associated with an isolated absorption band can be used to determine the strength of that band[28,29] and hence is useful for comparison with IR and microwave data in the overlap region. The information obtained by these methods can be used to study such systems as

a) ion-ion or ion-molecule interactions in tetra alkyl or metal salt solutions[30]
b) hindered rotational and translational motion of polar[31,32,33,34] and non-polar[35,36] liquids
c) the absorptions arising due to the formation of electron donor-acceptor complexes[37]

Refractive Index determination using a Michelson Interferometer

When operating an interferometer in the normal (non dispersive) mode the two beams recombining at the beam-splitter differ only by the phase lag caused by the displacement of the moving mirror. The interference pattern that arises is due to the phase shift undergone by one beam. A beam of electromagnetic radiation passing through a piece of dielectric

Fig. 3.1 Diagram showing dispersion in an absorption band

axation
ocess

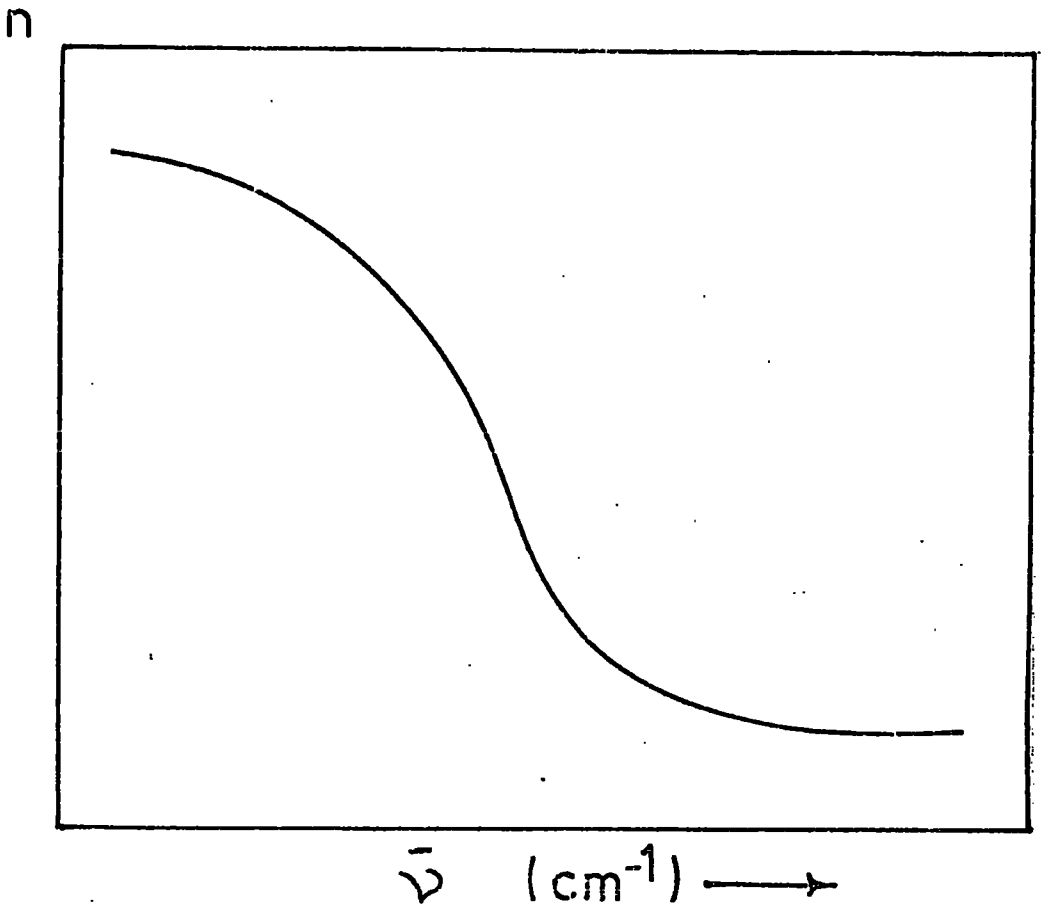

sonance
rocess

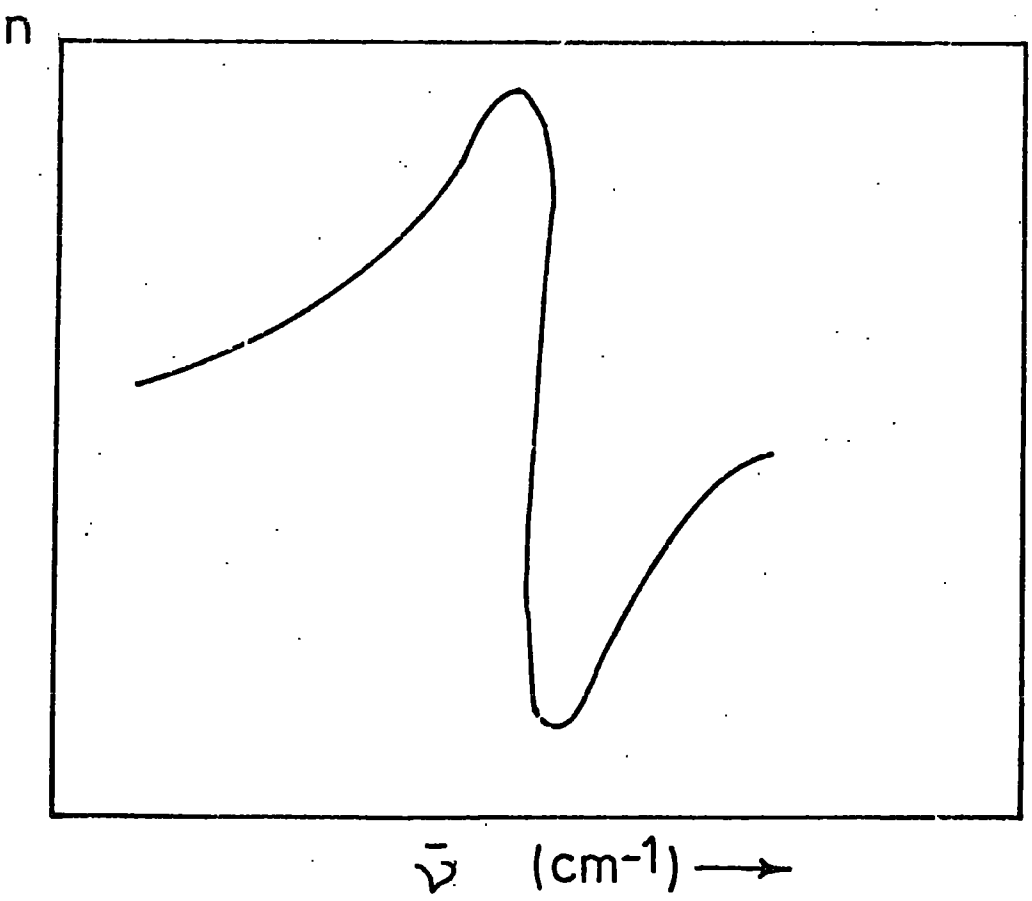

material also undergoes a phase shift which in this case is equal to $2\pi(n-1)d\bar{\nu}^2$ (where d = thickness of dielectric and n = refractive index of dielectric) compared to same beam in a vacuum. Therefore if a piece of dielectric material is inserted into one beam of the interferometer the effect is to optically displace the mirror and cause an additional phase shift. If the sample in the beam is non-dispersive, i.e. where n is constant for all frequencies of radiation, the grand maximum of the interferogram will be displaced by 2(n-1)d and hence the refractive index can be calculated directly from this shift (see figure 3.2). With a dispersive material in one arm of the interferometer the additional optical path length resulting from the sample is no longer independent of frequency. The combination of the differently displaced components of the beam result in the interferogram being asymmetrical as well as displaced (figure 3.2). The average optical path difference due to the sample can be taken from the interferogram as the displacement $\bar{x}$ from x = 0. This can be used to define a mean refractive index $\bar{n}$ by the relation

$$\bar{x} = 2(\bar{n} - 1)d \qquad 3.1$$

where d = thickness of the sample

The path difference due to the sample at a frequency $\bar{\nu}$ is given by the similar relation

$$\Delta(\bar{\nu}) = 2(n(\bar{\nu}) - 1)d \qquad 3.2$$

Due to the imperfections of the interferometer itself there is a small residual phase-difference given by

$$\phi_o(\bar{\nu}) = 2\pi\bar{\nu}\delta_o(\bar{\nu}) \qquad 3.3$$

where $\delta_o(\bar{\nu})$ is the small path difference corresponding to the residual phase-difference.

Fig. 3.2 Interferograms showing displacement and distortion arising from a sample in one beam

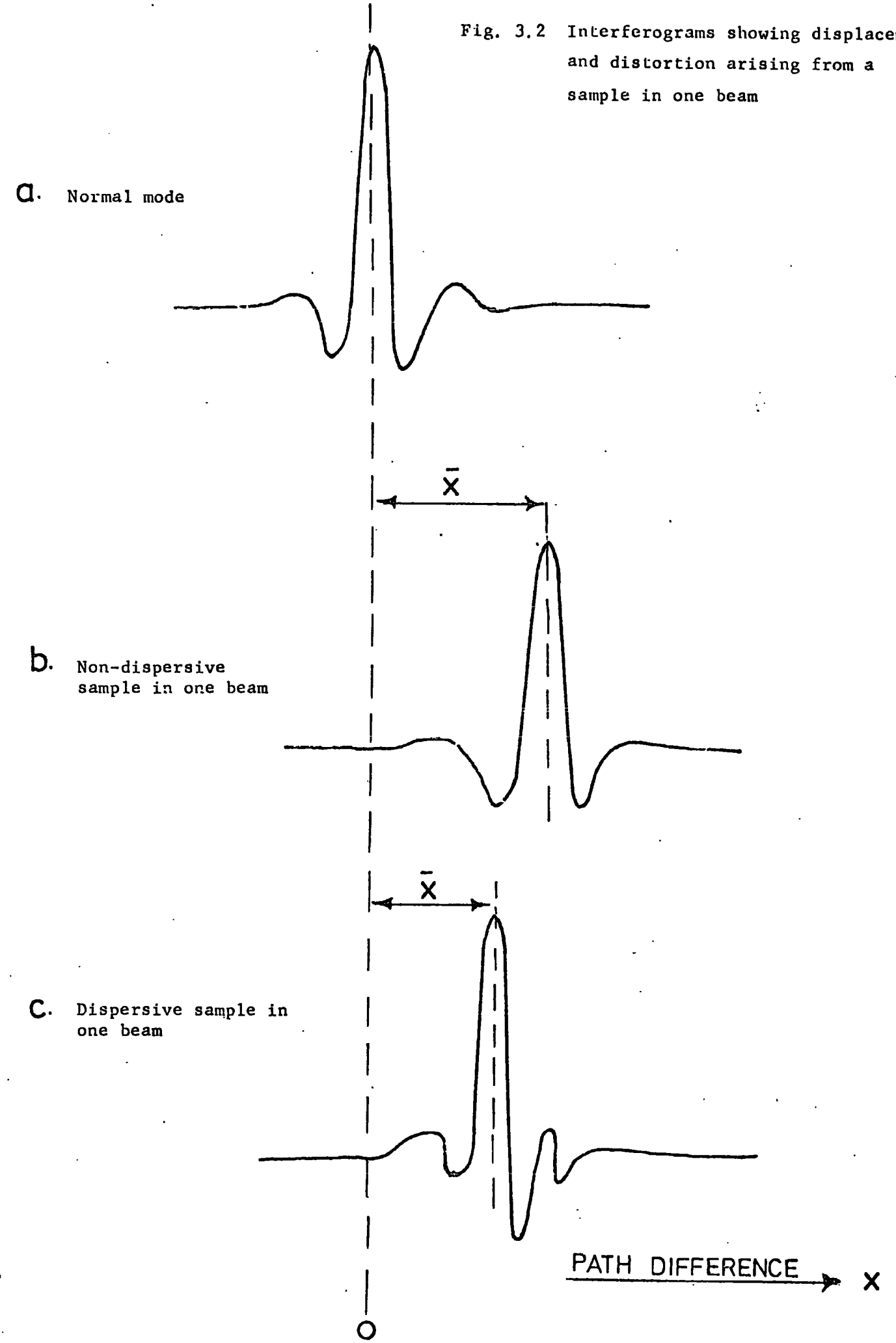

By consideration of the electric vectors[38] it can be shown that

$$\Phi(\bar{\nu}) = 2\pi\bar{\nu}[\Delta(\bar{\nu}) + \delta_o(\bar{\nu})] \qquad 3.4$$

The refractive index at frequency $\bar{\nu}$ is given, from equations 3.2, 3.3 and 3.4 by

$$n(\bar{\nu}) = 1 + \frac{1}{4\pi\bar{\nu}d}\,[\phi(\bar{\nu}) - \phi_o(\bar{\nu}) + 2m\pi] \qquad 3.5$$

where m = an integer

and $\phi(\bar{\nu})$ is the principle value of the true phase-difference

$$\Phi(\bar{\nu}) = \phi(\bar{\nu}) + 2m\pi \qquad 3.6$$

given by 3.4. where $-\pi < \phi(\bar{\nu}) \leqslant \pi$

In practice the calculation is awkward unless m = 0. To simplify the conditions the origin of computation is shifted to x, the displaced maximum. The real and imaginary parts of the transform are now

$$P(\bar{\nu}) = \int_{-\infty}^{+\infty} F(x)\cos 2\pi\bar{\nu}x\,dx = \rho(\bar{\nu})\cos\Psi(\bar{\nu})$$

$$Q(\bar{\nu}) = \int_{-\infty}^{\infty} F(x)\sin 2\pi\bar{\nu}x\,dx = \rho(\bar{\nu})\sin\Psi(\bar{\nu}) \qquad 3.7$$

and the refractive index is given by

$$n(\bar{\nu}) = 1 + \frac{\bar{x}}{2d} + \frac{1}{4\pi\bar{\nu}d}\,[\psi(\bar{\nu}) - \phi_o(\bar{\nu}) + 2m\pi] \qquad 3.8$$

where

$\phi_o(\bar{\nu})$ = instrument contribution

$\psi(\bar{\nu})$ = principle value of the phase difference $\Psi(\bar{\nu})$ such that $-\pi < \psi(\bar{\nu}) \leqslant \pi$

(NB $\frac{\bar{x}}{2d}$ = constant part of 3.8)

For the condition m = 0 the relation

$$|2[n(\bar{\nu}) - \bar{n}]d| < \tfrac{1}{2}\lambda \qquad 3.9$$

must be satisfied. Therefore the optical thickness $n(\bar{\nu})d$ must not depart by more than $\frac{1}{4}\lambda$, at any wavelength $\lambda = {}^{1}/\bar{\nu}$ of interest, from a mean optical thickness $\bar{n}d$. (Note that m may take other integer values to enable optically thicker samples to be studied). To eliminate systematic errors arising from instrument imperfections, equation 3.8 can be re-written with a background phase subtraction as

$$n(\bar{\nu}) = 1 + \frac{\bar{x}}{2d} - \frac{1}{4\pi\bar{\nu}d}\left[\underbrace{\left(\arctan\frac{Q(\bar{\nu})}{P(\bar{\nu})}\right)}_{\text{SAMPLE}} - \underbrace{\left(\arctan\frac{Q'(\bar{\nu})}{P'(\bar{\nu})}\right)}_{\text{BACKGROUND}} + m\pi\right]$$

where

Sample $Q(\bar{\nu})/P(\bar{\nu})$ includes cell and instrument residual phase errors

Background $Q'(\bar{\nu})/P'(\bar{\nu})$ is the solvent or empty cell and includes residual phase errors.

b) Design and Practical use of Cell

Refractive index determinations with a Michelson interferometer have usually been done with the instrument in such a configuration that the fixed mirror is horizontal.[39] The liquid or solid sample is then gravity held behind a sealing vacuum window (necessary in the case of liquid only) and the instrument run in normal manner. In order to determine refraction spectra with our instrument (a Beckman RIIC FS720) it was necessary to design a cell which could be mounted on its side and be easily filled. It was also essential to include some facility for quickly determining the true zero-path position in order to calculate the mean refractive index $\bar{n}$. Figure 3.3. shows a diagrammatic representation of the cell designed and constructed for use in this work.

The front window B is mounted against the teflon spacer C and sealed into the frame D. The window is then sealed against the spacer by the 'O' ring F. The assembled frame is mounted against the gold plated glass mirror, A, and held by 3 screws from the back. The cell is mounted slightly off axis in order to accommodate the small reference mirror G which can be covered by the shutter H when not in use. The entire cell is mounted into a frame on the instrument by two quick release clips. This frame also holds the vacuum window which is supported by a wire grid as shown in figure 3.4a. Once mounted the cell can be filled and emptied by means of the two teflon tubes T. This eliminates the need for demounting which would lead to loss of optical alignment. Figures 3.4b and c show the complete refractive index cell.

Special features of the cell described

The reference mirror G provides a very convenient means of finding the position of the true zpd and hence $\bar{x}$ and $\bar{n}$. Because the cell is

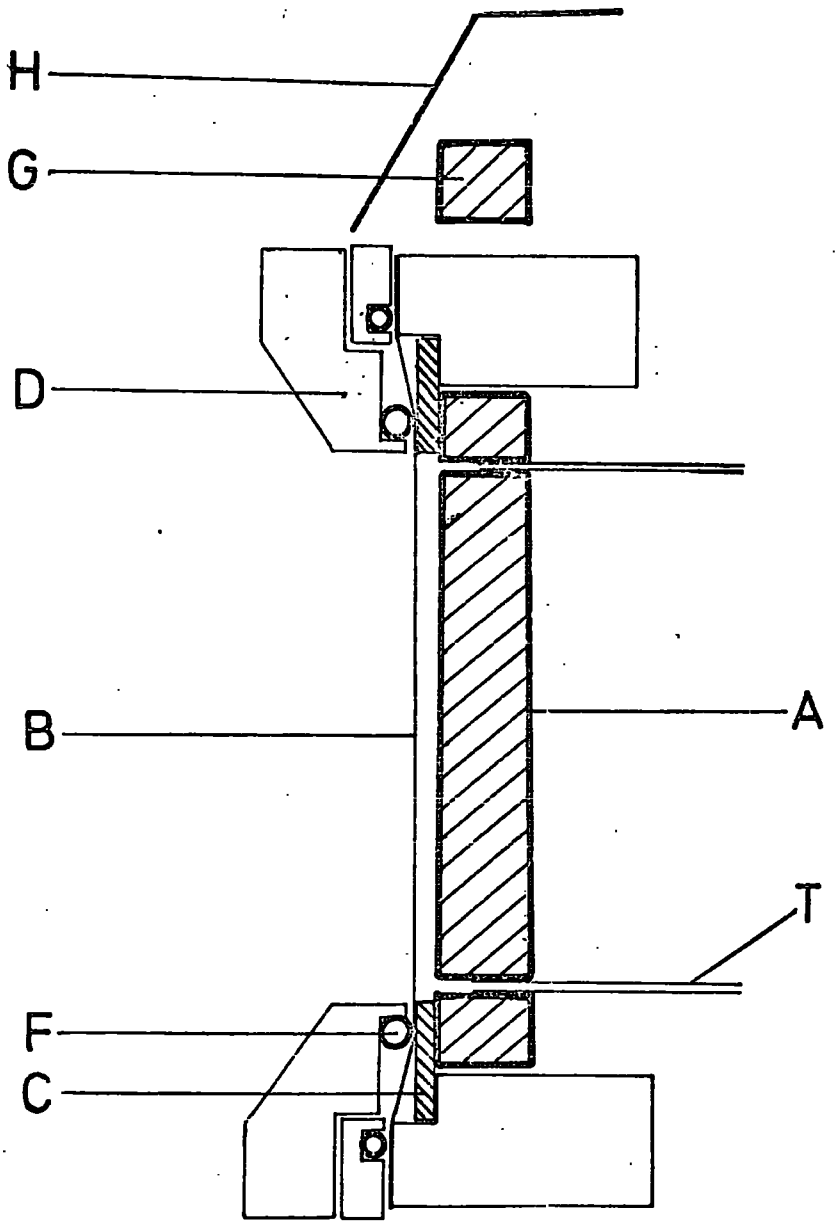

Fig 3.3

Diagrammatic section through refractive index cell.

b)

a)

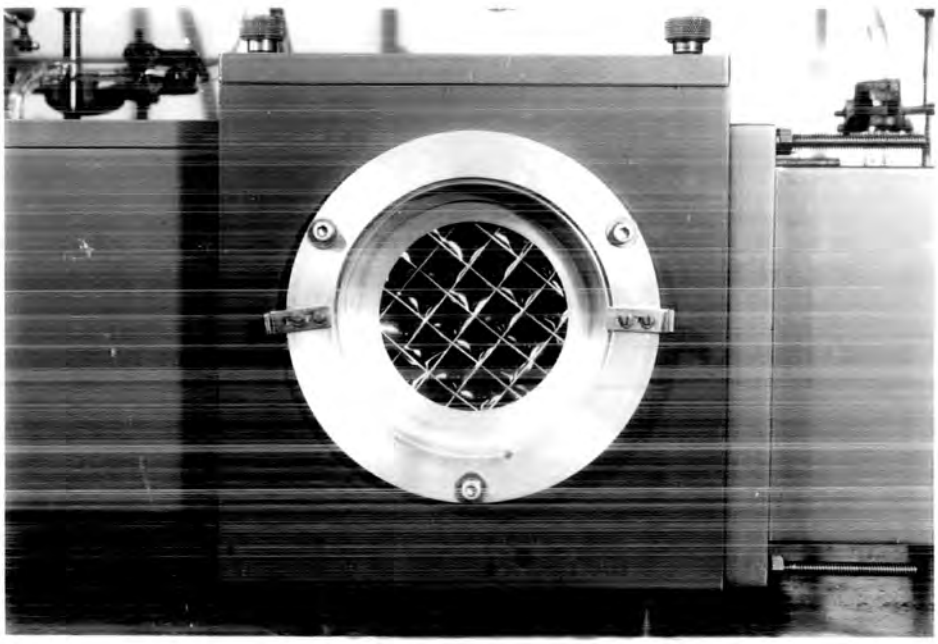

c)

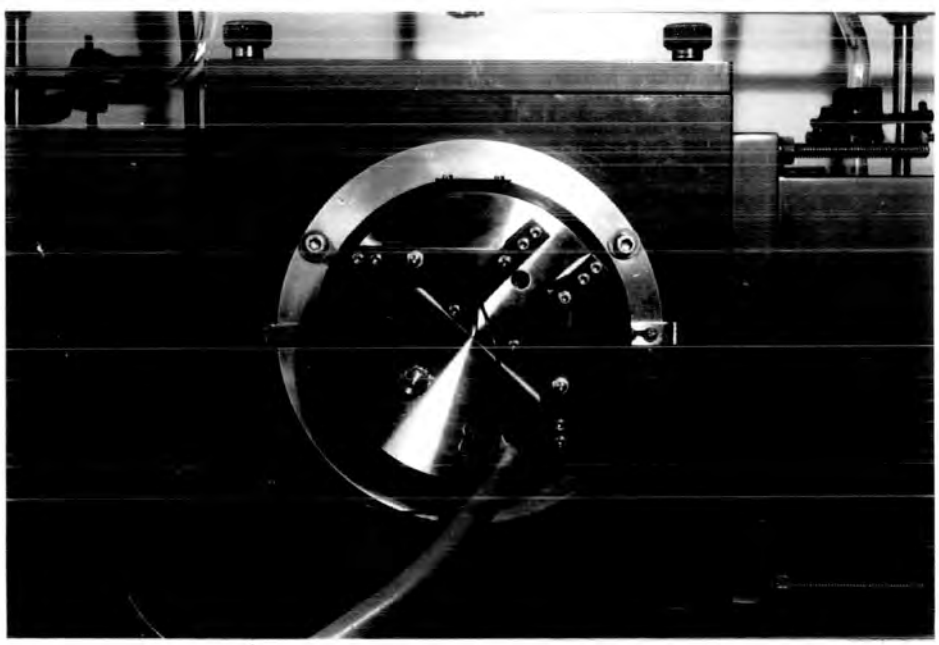

Fig. 3.4 Photographs showing a) the wire grid vacuum membrane support, b) the complete cell, c) the cell in position

sealed with a window it is possible to study many volatile corrosive and toxic materials which could not normally be allowed exposure in a laboratory (or instrument). Another advantage is that very thin samples can be contained in the cell where normally (for a gravity held liquid) the thickness of the sample will be limited by surface tension and viscosity effects. This is particularly useful when the samples are very strongly absorbing in the region of interest. The presence of a top window in the cell also causes some disadvantages due to absorptions, and more seriously reflections which both lead to distortion and a loss of modulation. These problems are discussed fully in section 3c.

Practical Operation

Before mounting the cell into the holder the instrument was tested for vacuum tightness and the supporting grid moved to such a position that the crossed wires did not obscure the small reference mirror. A similar wire grid was placed in the other arm to compensate for loss of modulation due to reduction of energy in one beam. The cell was fitted with standard Beckman R11C cantilevers which allow the optical alignment to be carried out in the manner described.[15] The initial optical alignment was carried out with the front window B removed so that the intensity of the undistorted interferogram could be maximised. Serious misalignment was corrected in the normal way, using the cross haired source apature and the small viewing mirror, as described in the instrument manual. After optimising the optical alignment the cell module can be removed from the mounting bracket, the window refitted and the complete cell remounted without seriously altering the alignment. A final adjustment was usually made immediately prior to operation.

During operation the space between the cell window and the vacuum membrane (about 1cm) was flushed with dried nitrogen to eliminate atmospheric water vapour.

The cell was filled through the bottom teflon tube T with a syringe. It was found that the thin window (12μM) of the cell 'bows' considerably during filling, especially when using a very viscous liquid such as tetrabromoethane. This 'bowing' causes divergence of the reflected light due to the liquid acting as a lens and leads to a serious decrease in modulation. To overcome this problem it was necessary to allow the cell to overflow, from the top tube T, for about 10-15 minutes so that the front window could flatten out. More serious 'bowing', which could not be cured by this method was normally associated with a trapped or twisted overflow tube. Damaged tubes were easily removed and new tubing araldited into the back of the mirror after etching the surface with fine abrasive paper (this is necessary because araldite will not readily adhere to teflon).

The modulation depth of the interferogram when operating in the dispersive mode is considerably less than in the normal mode and so nearly all runs were done with the maximum off set voltage (3v on RIIC Ltd. FS200 electronics) and high gain to make best use of the full dynamic range of the A/D and therefore obtain the best signal to noise ratio.

It was found after using the cell for long periods (1 week continuously) with liquid tetrabromoethane that the mirror surface began to deteriorate and flake off leading to a loss of modulation. The gold coating was easily replaced by vacuum evaporation in our applied physics department after removing the old coating with a potassium iodide/ iodine etch and cleaning the glass surface.

c) Results

Figure 3.5 shows some typical interferograms recorded with the cell using the cooled bolometer described in chapter 2. The fringes can be correlated with the ray diagram shown in figure 3.6 which represents some of the reflections possible in the cell. The fringes are easily assigned to cell reflections by the use of equation 3.1 which becomes

$$\bar{x}_{total} = \bar{x}_w + \bar{x}_s \qquad 3.11$$

from

$$\bar{x}_w = 2(\bar{n}_w - 1)d_w$$

where $\bar{x}_w$ = optical displacement due to window

$\bar{n}_w$ = mean refractive index of window

d_w = thickness of window

and

$$\bar{x}_s = 2(\bar{n}_s - 1)d_s$$

where $\bar{x}_s$ = optical displacement due to sample

$\bar{n}_s$ = mean refractive index of sample

d_s = thickness of sample

In the case of the empty cell $\bar{n}_s$ is taken to be one and hence the cell dimensions can be easily calculated from the chart interferogram. The interferograms were calibrated manually by marking off the 8μ punch intervals for a distance of at least 1000μ mirror drive which corresponds to about 5cm chart drive. This method was found to be very accurate due to the fact that the drive speed of the chart and mirror were constant.

An additional feature which was used in the assignment of the interferogram features is shown by fringes 3,4, 8 and 9, which appear negative (dark) with respect to the rest of the fringes. This is due to

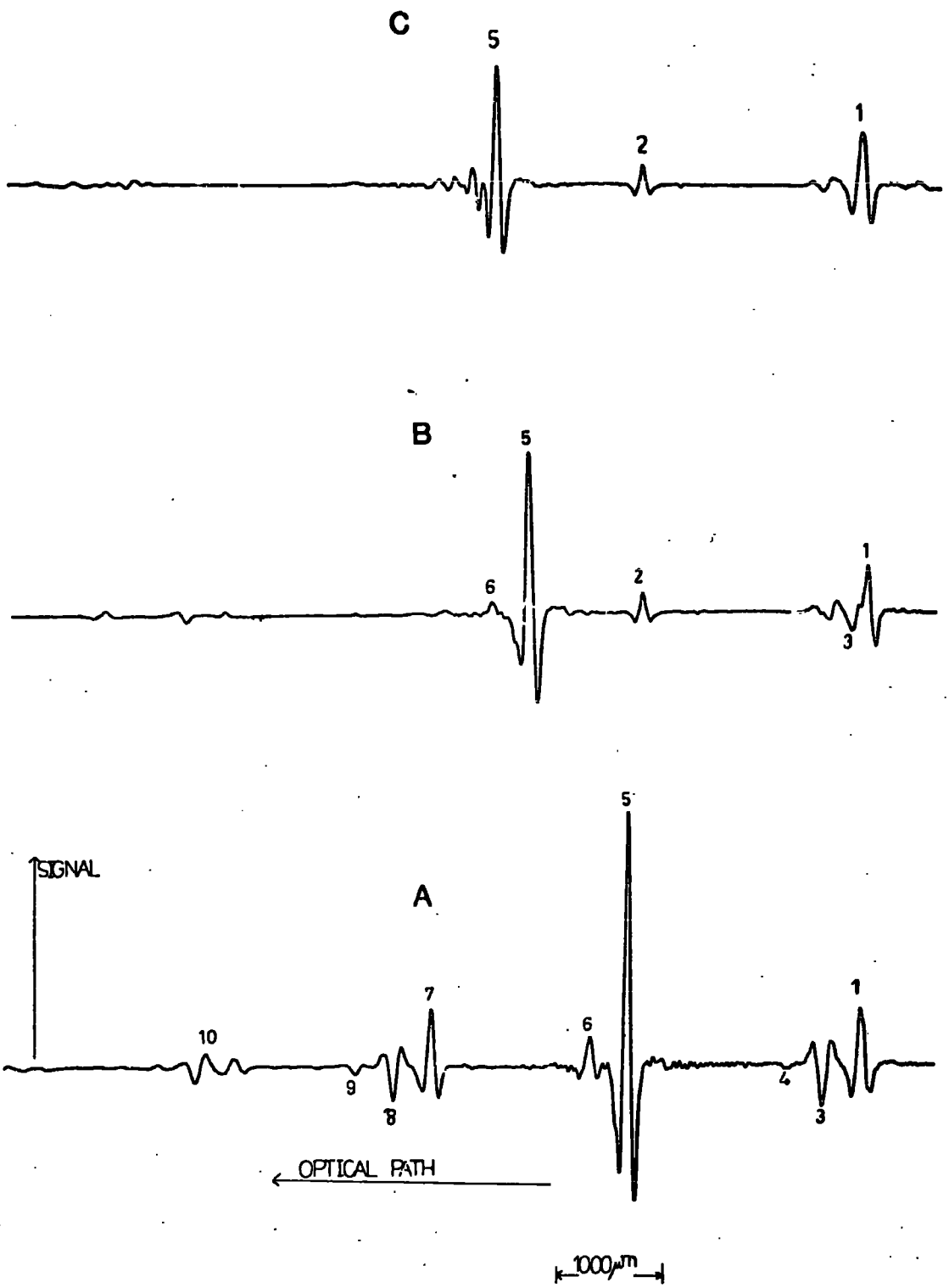

Fig. 3.5 Interferograms recorded from the refractive index cell with the cooled detector

A) empty cell

B) liquid p.difluorobenzene

C) liquid tetrabromoethane

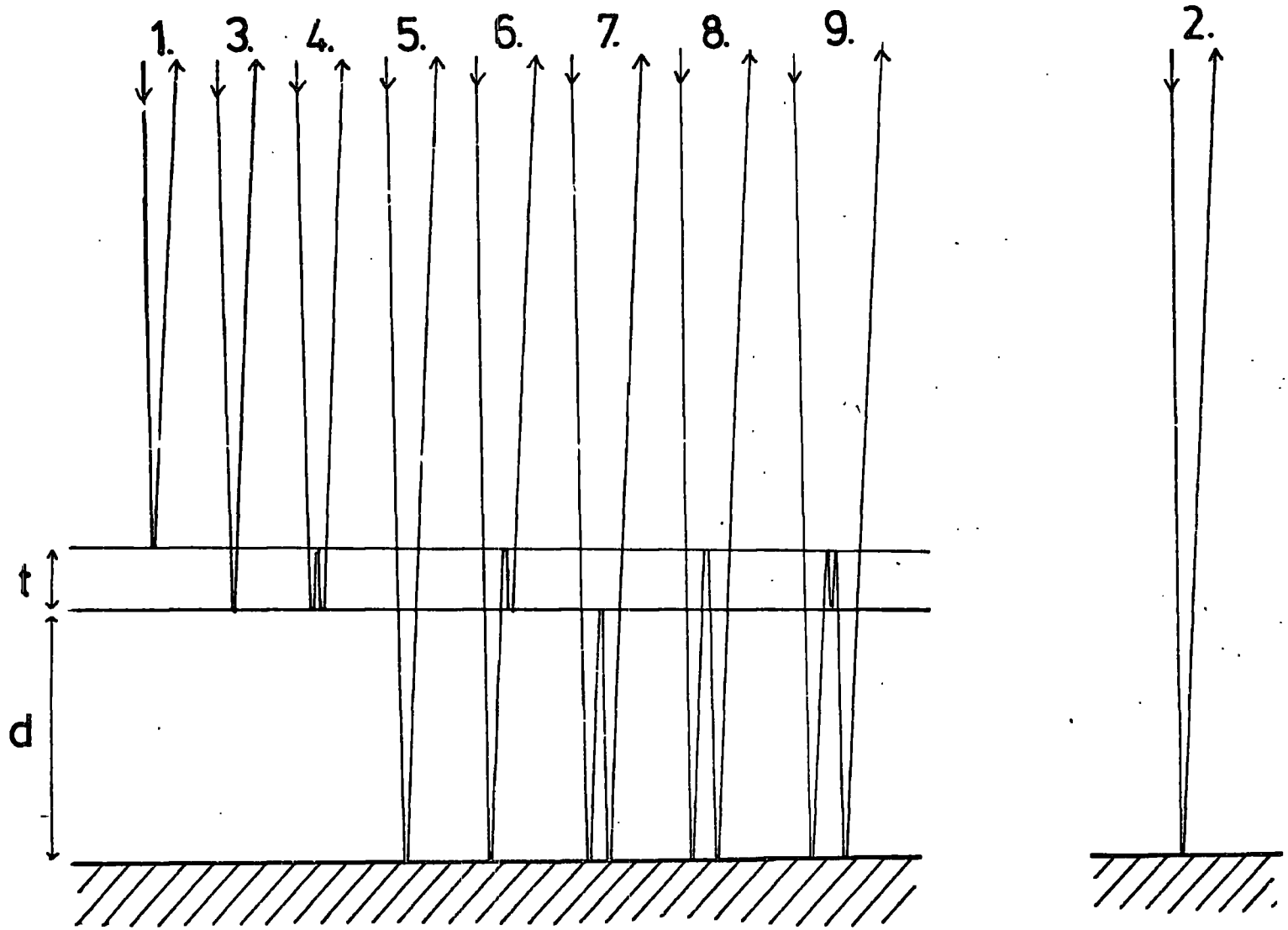

Fig3.6 Ray diagram showing origin of fringes observed in interferograms.

the phase change of π associated with a reflection with a more optically dense medium from a less opitcally dense medium which does not occur when the reflection is from the less optically dense medium (hence out of phase and appears dark). Table 3.1 shows the optical path differences in the cell, relative to the top window reflection (1), and a comparison with calculated values. Table 3.2 shows some of the important fringe spacings which are used to determine the cell dimensions and parameters necessary for the refractive index determination. From figure 3.5 it can be seen that the length of interferogram which can be conveniently transformed lies between fringes (3) and (7). This distance is determined by the thickness of the cell d and the optical thickness of the sample. In order to obtain reasonable phase resolution it was necessary to optimise the sample thickness. A very thick sample leads to poor modulation and hence a low signal/noise ratio and conversly a very thin sample means poor resolution due to the short distance (3)→(7) (see Chapter I). However, it is possible to edit these features before computation. The simplest way to do this is to reproduce the interferogram onto cards and then replace between (7)-(9) and (1)-(3) with constant values. A similar process could be carried out on a computer terminal (VDU) which would eliminate the punching of extra cards. A third attempt has been made to edit the data in the following way. The punched tape is read into a small data processing computer (Varian 620/L and then displayed on an oscilloscope. By means of a small moving marker, also displayed on the scope, the points between which editing is necessary can be pinpointed and the values punched out on the terminal. These values can then be read into a suitably modified Fourier transform phase calculation program so that the editing is done internally. So far results have only been obtained for manual editing which has not been completely successful due to the presence of fringe (6). Unfortunately it

Table 3.1 Optical Path Differences of observed fringes relative to reflection from top surface of cell window (feature (1) in figures 3.5 and 3.6)

Fringe	Phase Change[a]	Optical Path Difference	Recorded[c] path difference(μ)	Predicted path difference[b,c](μ)	Error %
2[d]	π	$2d+2t$	2090	2056	1.6
3	0	$2t+\bar{x}_\omega$	355	357	0.6
4	0	$4t+2\bar{x}_\omega$	696	713	2.5
5	π	$2t+2d+\bar{x}_\omega+\bar{x}_s$	2183	2209	1.2
6	π	$4t+2d+2\bar{x}_\omega+\bar{x}_s$	2528	2565	1.5
7	3π	$2t+4d+\bar{x}_\omega+2\bar{x}_s$	4026	4061	0.9
8	2π	$4t+4d+2\bar{x}_\omega+2\bar{x}_s$	4378	4417	0.9
9	2π	$6t+4d+3\bar{x}_\omega+2\bar{x}_s$	4736	4774	0.8

a. A π-phase change means that fringe is bright. Zero phase change means that fringe is dark (NB $2\pi = 0$, $3\pi = \pi$).

b. These predictions are based on, $t = 102\mu$ (measured). $\bar{n}_\omega = 1.748 \pm 0.015$ and $d = 926 \pm 4\mu$ are the average values from eight interferograms. (Compression of the spacer in the cell reduces d from $\approx 980\mu$ to this value).

c. For empty cell (3.5A).

d. This fringe is not observed on 3.5A because it is too close to fringe 5. The recorded value is from 3.5B and C.

Table 3.2 Fringe spacings used for the determination of cell dimensions and refractive indices

Fringes	Optical path Difference	Comments
3 - 7	$4d + 2\bar{x}_s$	Length of interferogram which can be conveniently transformed
1 - 3	$2t + \bar{x}_\omega$	Used to calculate $\bar{n}_\omega$
7 - 8	$2t + \bar{x}_\omega$	" " " "
5 - 6	$2t + \bar{x}_\omega$	" " " "
3 - 5	$2d + \bar{x}_s$	Used to calculate d when $\bar{x}_s = 0$ (empty cell)
5 - 7	$2d + \bar{x}_s$	" " " " "
2 - 5	$\bar{x}_s + \bar{x}_\omega$	Used to calculate $\bar{n}_s$ when $\bar{x}_\omega$ known

is not possible to remove fringe (6) by an editing technique because it lies too close to the main fringe (5) and can be moved only by changing the window thickness. Even though it is partially removed (or possibly over-removed) by the subtraction of a background phase function there still seems to be some noise associated with it. To eliminate this feature the possibility of using anti-reflecting coatings[40,41] was considered but it was decided that the limited frequency range over which they are effective would not give any significant improvement. Attempts were made to scatter the reflected radiation by scoring both surfaces of the top window with different grades of abrasive paper. This method was completely unsuccessful due to the fact that the wavelength of the incident radiation was too long. Interferograms from two different thicknesses of sample were run in an attempt to remove the feature by subtraction. Unfortunately this method has failed because the intensity of fringe (6) is directly dependent on fringe (5), hence any suitably weighted subtraction which completely removes fringe (6) also removes fringe (5). An attempt is to be made in the future to obtain a record of this feature on its own by the subtraction of the uncovered mirror interferogram from a normal empty cell interferogram. There are then two possibilities to be examined if this can be done.

(i) It may then be possible to subtract the single feature from the sample interferogram after adjusting the intensity with a scaling factor determined from the amplifier gain setting.

(ii) It may be possible to ascertain the shape function of the feature and subtract it from the phase spectra after calculation.

Finally it has been found that some window materials, notably polythene, give rise to less intense reflections and hence cause less of a fringe (6) problem as well as improving the fringe (5) modulation

due to their increased transmission. Experiments are being carried out on other available materials to find something with even better transmission characteristics in this region.

Figure 3.7 shows the dispersion curve of tetrabromoethane recorded using the cell described and the cooled detector with a 100 guage beam-splitter. A background phase spectrum of the empty cell was subtracted from the sample phase spectrum. Because the fringe spacing 3-7 is small for an empty cell the phase resolution is background limited to ~ 10 cm^{-1}. The curve has not been drawn through the point of 146 cm^{-1} because this is thought to be a feature arising from the transformation of fringe 6. The refractive index at 29.7 cm^{-1} is 1.670 which is within 1.6% of the laser determined[42] value of 1.643 at this frequency. The average experimental measurement error from table 3.1 is 1.25% which would lead to a maximum error of 2.5% in the final dispersion curve (due to subtraction of background). However, all of the dispersion curves recorded to date have been higher than the expected level (from laser measurement) which suggests that the error is systematic.

The small feature at 34 cm^{-1} has been found to be reproducible and can be correlated with a small absorption in this region (see figure 2.24). This feature has not been observed previously[39] and it is probably visible because of the higher sensitivity of the cooled detector compared to the Golay cell at low frequency. The position of the other bands compare favourably with the literature[39] and the absorption spectrum (except for the absence of the band at 55 cm^{-1}) but because of the low phase resolution a detailed analysis of the band intensities has not been carried out.

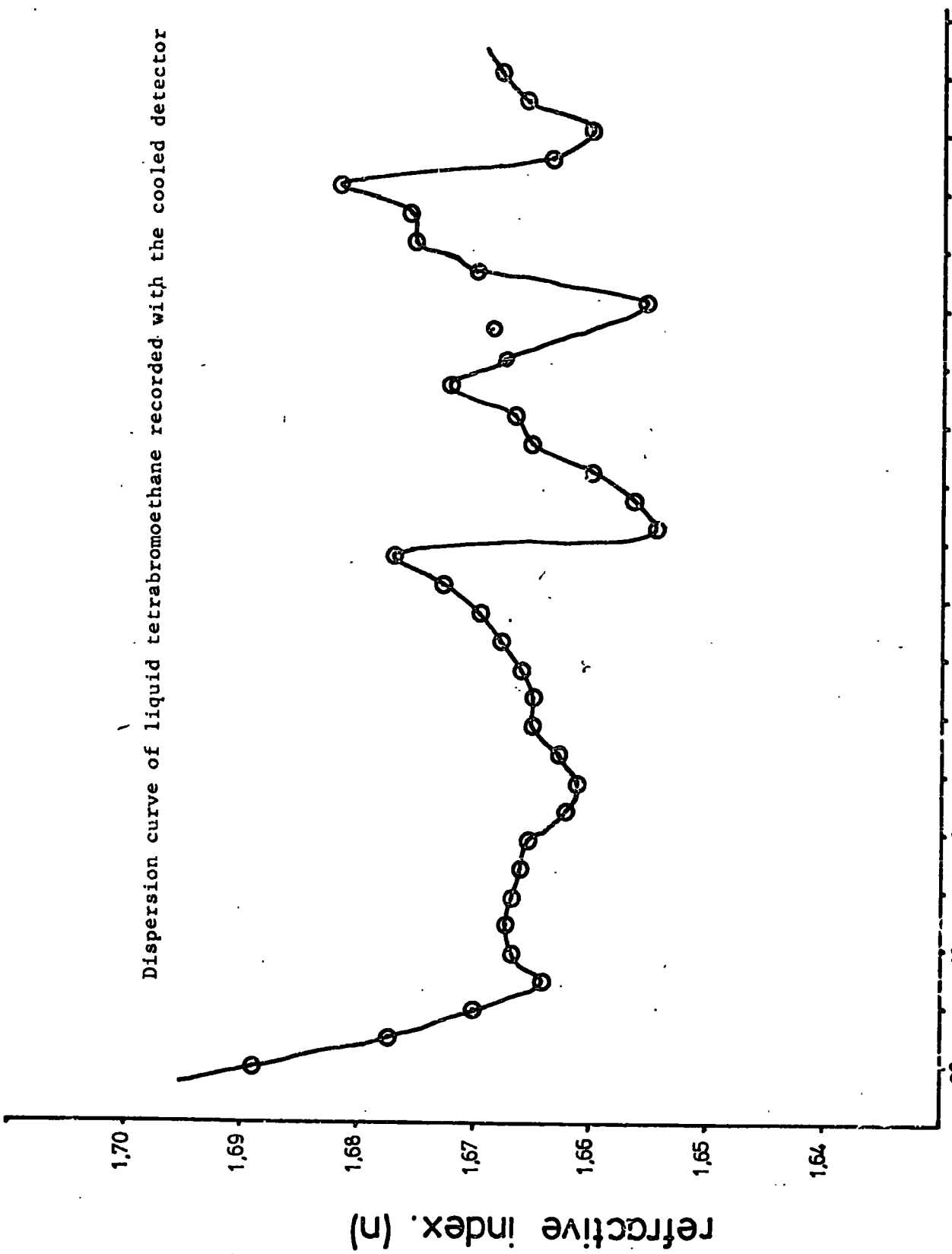
Dispersion curve of liquid tetrabromoethane recorded with the cooled detector
refractive index. (n)
1,70
1,69
1,68
1,67
1,66
1,65
1,64
20
40
60
80
100
120
140
160
180
200
frequency. (cm^{-1})

Fig 3.7

CHAPTER IV

Proposals for future work

In order to make the best use of the instrument modifications described in this thesis and therefore make the original studies proposed in Chapter I, it is necessary to overcome the technical problems which have arisen.

The high frequency altennation at $\sim 120\ cm^{-1}$ when operating in the polarising mode is at present thought to arise from a 'software' problem and investigations are currently being carried out into the effects of the subtraction of different 'mean levels' during the computation. When this problem has been solved the frequency range of this system should be up to about $\sim 150\text{-}200\ cm^{-1}$ which will make it possible to study complete broad bands more accurately than was possible previously.

Attempts must be made to quickly and accurately edit the unwanted reflection fringes from the refractive index cell data. In particular the fringe 6 (referring to chapter 3) must be removed before the dispersion spectra can be analysed in detail. When the cell has been proved to give accurate results it will be possible to make original studies in the far-infrared region and correlate dispersion data with intensity data as proposed in chapter 1.

The results obtained from tests on the cooled detector have indicated that the bolometer element may not be operating at its 'optimum' temperature of 1.5K due to the heating effect of the mercury source lamp. In order to accurately control the amount of radiation reaching the element a small adjustable iris is to be fitted over the detector light

guide. It will then be possible to study the heating effect of the radiation and operate the bolometer at its optimum temperature, hence obtaining the maximum sensitivity possible with this detector.

In order to take advantage of the high speed of response of the cooled detector the electronics are being modified so that there will be facilities for operating with different sampling intervals and time constants. This will make it possible to collect the data up to about five times faster than at present (the data collection speed will then be limited by the paper tape punch). In addition to this the present electronics only operate on half-wave rectification which means that half the signal is lost. Therefore the conversion of the amplifier to full-wave rectification will effectively increase the signal intensity recorded and facilitate the study of optically thicker, more absorbing samples such as the biochemical systems described (chapter 1).

Finally it is proposed that a reflectance module be constructed for the study of the reflectance and transmission spectra of metal, metal oxide and zeolite surfaces, and of gases adsorbed onto such materials, in the far-infrared region. By this method the nature and extent of the bonding of the material to the potential catalyst surface can be studied. Reflection studies of this type have been made at short wavelengths by the use of integrating spheres[43] but the 360^{o} radiation collection becomes very difficult at long wavelengths, partly due to a lack of highly reflective surface coatings. Tests are to be carried on $\sim 120^{o}$ collection from polished aluminised mirrors in order to try to achieve better signal-to-noise ratios than those obtained by straight forward transmission methods.

References

1. D.H. Martin and E. Puplett, Infrared Physics, 10, pp105-109, (1969).
2. G.W. Chantry, 'Submillimetre spectroscopy', Academic Press (1971), p113 →
3. C. Barker and J. Yarwood, J.C.S. Faraday II (1975) vol. 71, p1322.
4. J.C. Evans, G.Y.S.Lo, J.Phys.Chem. 69, 1965, 3223.
5. Biological Membranes (Ed. D. Chapman) Academic Press, 1964, Chap.4.
6. Transport phenomena in Bio membranes, N. Lakshminarayanaiah, Academic Press 1969.
7. Proceedings of 'Symposium on Calcium and Cellular Function' (Ed. A.W. Cuthbert) McMillan, 1970.
8. P.A. Lambert, I.C. Hancock, J. Baddiley, Bicchem J. (1975), 149, pp519-524.
9. J. Baddiley, Essays in Biochem. 8, (1972), pp35-77.
10. Water, A comprehensive treatment (Ed. F. Franks) Plenum Press, London 1973, Vol.3, Chap.4, Vol.1, Chap.5.
11. M.A. Gebbie and R.Q. Twiss, Reports on progress in Physics (1966), Vol.29, pp729-756.
12. J. Chamberlain, G.W. Chantry, N.W.B. Stone, Chem.Soc.Rev. 4, 1975, pp569-588.
13. Ref. (2) p.50.
14. See for example R.J. Bell, Academic Press, 1972.
15. FS720 Manual RIIC 1967.
16. J. Yarwood, 'Absolute Intensity Measurements in the region 10-600 cm^{-1}, Beckman-RIIC Ltd. Monograph.
17. R.A. Smith, F.E. Jones, R.P. Chasmar, The detection and measurement of infra-red radiation, Oxford University Press, 1968.
18. R.C. Jones, J.Opt.Soc.Am. 1953, 43, pp1-14.

19. E.H. Putley, D.H. Martin, Spectroscopic Techniques, Chap.4, North Holland Publishing Company, 1967.

20. M.F. Kimmet, Far infrared Techniques, London Pion Ltd. 1970, Chap.4.

21. E.H. Putley, Advances in Geophysics, 1970, 14, p129.

22. Q.M.C. Bolometer Handbook.

23. F.J. Low, J.Opt.Soc.Am. 1961, 51, 1300.

24. Dr. P. Ade, Q.M.C. Physics Dept. Personal Communication.

25. Q.M.C. IRL. Polarising Interferometer Conversion Handbook.

26. Refers to FS200 circuit diagram C1570/1, Golay Amplifier and demodulator.

27. J. Chamberlain, Chem.Phys.Lett. 1968, Vol.2, No.7, p464.

28. J. Chamberlain, Infrared Physics Vol.5, 175-178, 1965.

29. G.W. Chantry, ref. 2, p.114.

30. J. Yarwood and C. Barker, J.Chem.Soc. Faraday Trans. II, 71, 1322 (1975).

31. M.M. Davies, G.W.F. Pardoe, J.E. Chamberlain and H.A. Gebbie, Trans Faraday Soc. 64, 847, (1968).

32. G.W.F. Pardoe, Spectrochimica Acta, 27A, 203, (1971).

33. A. Gerschel, I. Darmon, C. Brot, Mol.Phys. 23, 317, (1972).

34. H.I. Baise, J. Chem.Soc., Faraday II, 68, 1904, (1972).

35. G.J. Davies, J. Chamberlain and M.M. Davies, J.Chem.Soc., Faraday Trans. II, 69, 1278, (1973).

36. G.W.F. Pardoe, J.Chem.Soc. Trans. Faraday Soc., 66, 2699, (1970).

37. The spectroscopy and Structure of Molecular Complexes (Ed. J. Yarwood) Plenum Pub.Co. London, 1973, p124 and 262-4.

38. J. Chamberlain, J.E. Gibbs, H.A. Gebbie, Infrared Physics, 9, pp185-209, (1969).

39. J. Chamberlain, A.E. Costley, H.A. Gebbie, Spectrochimica Acta, 23A, pp2255-2260, (1967).

40. A. Vaško, Infrared Radiation, Iliffe Books Ltd., 1968, p141.

41. J. Yarwood and W.J. Orville-Thomas, J. Chem.Soc. Trans. Faraday Soc. 62, 3011 (1966), (Antimony trioxide was used to reduce reflection from a germanium Fabry-Perot etalon).

42. See for example ref. 2, appendix 4.

43. Produced by Beckman-RIIC Ltd.